Gondwana Research 111 (2022) 103–121

Contents lists available at ScienceDirect

Gondwana Research

journal homepage: www.elsevier.com/locate/gr

# Long-term Phanerozoic global mean sea level: Insights from strontium isotope variations and estimates of continental glaciation

Douwe G. van der Meer [a,b,*], Christopher R. Scotese [c], Benjamin J.W. Mills [d], Appy Sluijs [b], Aart-Peter van den Berg van Saparoea [e], Ruben M.B. van de Weg [a]

[a] CNOOC International, 90 Oxford Road, Uxbridge UB8 1LU, United Kingdom
[b] Department of Earth Sciences, Utrecht University, 3584 CB Utrecht, the Netherlands
[c] Department of Earth and Planetary Sciences, Northwestern University, Evanston, IL 60208, United States
[d] School of Earth and Environment, University of Leeds, Leeds LS2 9JT, United Kingdom
[e] Kallisto Geoscience, De Groene Haven 182, Delft, the Netherlands

ARTICLE INFO

*Article history:*
Received 25 September 2021
Revised 12 July 2022
Accepted 15 July 2022
Available online 04 August 2022
Handling Editor: M. Santosh

*Keywords:*
Eustasy
Tectono-Glacio-Eustatic
Phanerozoic
Glaciation
Sea level
Sequence stratigraphy

ABSTRACT

Global mean sea level is a key component within the fields of climate and oceanographic modelling in the Anthropocene. Hence, an improved understanding of eustatic sea level in deep time aids in our understanding of Earth's paleoclimate and may help predict future climatological and sea level changes. However, long-term eustatic sea level reconstructions are hampered because of ambiguity in stratigraphic interpretations of the rock record and limitations in plate tectonic modelling. Hence the amplitude and timescales of Phanerozoic eustasy remains poorly constrained. A novel, independent method from stratigraphic or plate modelling methods, based on estimating the effect of plate tectonics (i.e., mid-ocean ridge spreading) from the $^{87}Sr/^{86}Sr$ record led to a long-term eustatic sea level curve, but did not include glacio-eustatic drivers. Here, we incorporate changes in sea level resulting from variations in seawater volume from continental glaciations at time steps of 1 Myr. Based on a recent compilation of global average paleotemperature derived from $\delta^{18}O$ data, paleo-Köppen zones and paleogeographic reconstructions, we estimate ice distribution on land and continental shelf margins. Ice thickness is calibrated with a recent paleoclimate model for the late Cenozoic icehouse, yielding an average ~1.4 km thickness for land ice, ultimately providing global ice volume estimates. Eustatic sea level variations associated with long-term glaciations (>1 Myr) reach up to ~90 m, similar to, and is at times dominant in amplitude over plate tectonic-derived eustasy. We superimpose the long-term sea level effects of land ice on the plate tectonically driven sea level record. This results in a Tectono-Glacio-Eustatic (TGE) curve-for which we describe the main long-term (>50 Myr) and residual trends in detail.



**Contents**



* Corresponding author at: CNOOC International, 90 Oxford Road, Uxbridge UB8 1LU, United Kingdom.
*E-mail address:* douwe.vandermeer@intl.cnoocltd.com (D.G. van der Meer).

https://doi.org/10.1016/j.gr.2022.07.014
1342-937X/

## 1. Introduction

Traditionally long-term eustatic sea level curves have been based on stratigraphic analyses of marginal marine sediment sequences (e.g., Haq et al., 1987; Vail et al, 1977). When sequence stratigraphy first emerged, global mean sea level (GMSL), was posited to be the dominant controls on stratigraphic architecture in passive-margin settings (Vail et al, 1977). This has been shown to be a gross oversimplification in many subsequent studies, as summarized by Miall (2010). Also, discussions on sequence stratigraphy are more frequently described in terms of short-term eustatic patterns (few Myr or less), which is a key distinction from the derivation of long-term eustatic curves (i.e. Simmons et al., 2020). Other processes not discussed by Vail et al. (1977), such as local tectonics and geoid variations (Müller et al., 2008; Raymo et al., 2011; Sluijs et al., 2008; Stocchi et al., 2013) as well as glacial rebound (Farrell and Clark, 1976; Peltier and Andrews, 1976; Woodward, 1888) are now known to play significant roles (e.g., Miller et al., 2005).

Dynamic topography caused by mantle convection (Müller et al., 2008) also affects the regional signal of global sea level (eustasy) (Moucha et al., 2008) as well as sea level curves derived from continental or 'modern land' flooding (Marcilly et al. (2022). Kominz et al. (2008) estimated that up to 105.5 m (at 53 Ma) of apparent sea level fall along the coastal margin of New Jersey may be because of the subducting Farallon slab under North America. Though the Farallon slab is well-studied since its initial identification (Grand et al., 1997), slab sinking rates are still debated (i.e. Boschman et al., 2018; Butterworth et al., 2014; Liu et al., 2008; Sigloch and Mihalynuk, 2013; van der Meer et al., 2018). Consequently, estimates of dynamic topography (Burgess and Moresi, 1999; Liu, 2015; Müller et al., 2008; Spasojevic and Gurnis, 2012) are poorly constrained. Since it is difficult to assess the impact of these processes with any certainty, the isolation and reconstruction of eustasy from the stratigraphic record is complex and requires data from diverse, multi-regional settings. For these reasons, the overall amplitude of global Phanerozoic long-term sea level is not well-known.

As summarized in van der Meer et al. 2017, the most fundamental weakness of using the stratigraphic record to reconstruct global sea level in the past is the problem of equifinality, the notion that in open systems a given end state can be reached by many potential means (Von Bertalanffy, 1968). As Burgess and Prince (2015) demonstrated, it is likely that different forcing processes or combinations of forcing processes can produce very similar stratigraphic architectures. Burton et al. (1987) argued that the impact of a forcing process can only be quantified reliably if the impacts of all the other forcing processes are known. In other words, an unknown can only be determined reliably if all other parameters are known. If this is not the case, as in practically every natural system, assumptions must be made. This leaves room for substantial uncertainty and a high likelihood of equally plausible alternative scenarios that are consistent with the observations. The importance of quantifying, or at least constraining, all the forcing parameters as much as possible is clear. Until this can be done more precisely and reliably, it seems prudent to use reconstructions of eustatic sea level based on sequence stratigraphic interpretations as a reference to check the consistency of results rather than the primary source of information. A goal in the analysis of sedimentary basins is thus the development of a eustatic sea level model that is derived independently from sequence stratigraphic interpretations. More recently, the uncertainties and differing opinions of eustatic sea level reconstruction from sequence stratigraphy were reviewed by Simmons et al. (2020) and Wright et al. (2020).

To this end, as an alternative method of sea level reconstruction based on rock record observations (Fig. 1) (e.g. Hallam, 1984; Haq, 2018a, 2018b, 2014; Haq et al., 1987; Haq and Al-Qahtani, 2005; Haq and Schutter, 2008; Vail et al, 1977) plate tectonic modelling has been proposed as an alternative method to stratigraphic techniques to isolate and reconstruct long-term changes in eustatic sea level. Rates of mid-ocean ridge spreading determine the average age of the ocean floor and therefore, according to the depth/age relationship of cooling oceanic crust (Parsons and Sclater, 1977; Stein and Stein, 1992), control the volume of the ocean basins. Assuming a constant volume of sea-water and conservative estimates of continental hypsometry, the changing volume of the ocean basins directly dictates first-order mean eustatic sea level at > 10 Myr timescales (Conrad, 2013; Miller et al., 2005; Simmons et al., 2020; van der Meer et al., 2017). Improved plate tectonic models of the ocean basins during the Cenozoic and Cretaceous and increasingly detailed paleo-ocean age grids (Karlsen et al., 2020; Müller et al., 2019, 2016, 2008; Vérard et al., 2015), provide better constrained estimates of the volume of the ocean basins. However, because there is no oceanic crust for pre-middle Jurassic times, any estimates of long-term eustasy in the early Mesozoic and Paleozoic eustasy from plate tectonic reconstructions are, necessarily, entirely model-driven (Norton and Lawver, 2014; Torsvik et al., 2010).

The evolution of the Panthalassa (Paleo-Pacific) ocean, which comprises most of the oceanic crust that existed before the breakup of Pangea, is highly uncertain. Plate tectonic models generally describe the plate tectonic evolution of Panthalassa in terms of a 3 to 4 plate system (i.e., Wright et al. 2020). With relatively few spreading ridges and subduction along its perimeter, this plate tectonic scenario leads to relatively old, deep ocean crust resulting in a globally lower eustatic sea level. However, geological and tomographic evidence for intra-oceanic subduction zones show that Panthalassa was comprised of numerous, fragmented plates with a concomitant number of fast-spreading ridges and subduction zones (Boschman and van Hinsbergen, 2016; Domeier et al., 2017; Sigloch and Mihalynuk, 2013; van der Meer et al., 2012). This alternate geometry generates higher eustatic sea levels prior to the Cretaceous.

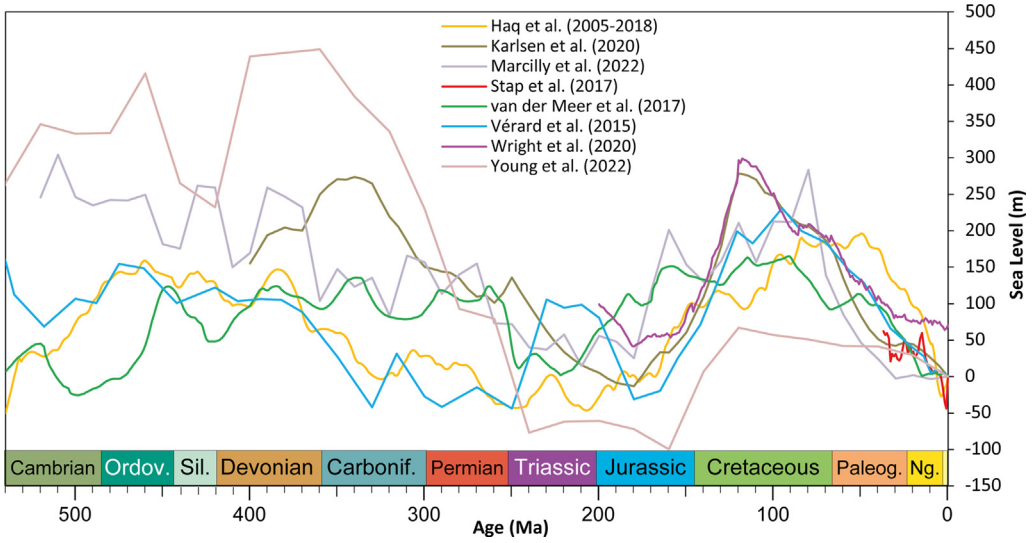


**Fig. 1. Phanerozoic long-term sea level reconstructions.** Eustatic sea level from plate tectonic models (Karlsen et al., 2020; Vérard et al., 2015; Wright et al., 2020; Young et al., 2022), strontium isotopes as a proxy for ridge spreading (van der Meer et al., 2017), 'modern land' flooding (Marcilly et al., 2022), a compilation of stratigraphically derived curves of Haq et al. (Haq, 2018a, 2018b, 2014; Haq and Al-Qahtani, 2005; Haq and Schutter, 2008) and from a Late Cenozoic ice/sea level paleo-climate model, 1 Myr averaged (Stap et al., 2017). As shown, estimates vary widely reflecting the large uncertainty in sea level reconstruction.

Though plate tectonics ultimately controls the volume of the ocean basins, the volume of the water in the ocean basins depends on the volume of water stored in continental ice sheets. During major icehouse periods in the Phanerozoic (Scotese et a., 2021), up to tens of million km$^3$, or several % of the global volume of water may be sequestered in continental ice sheets covering more than 30 % of the Earth's continents. The waxing and waning of continental ice caps can result in changes in global eustatic sea level of up to ~200 m in less than 100,000 years (e.g. (Davies et al., 2020; Miller et al., 2020, 2005; Rohling et al., 2014). Glacio-eustasy may even lead to up to 300 m of eustatic sea level changes on timescales > 1 Myr (Davies et al., 2020). Long-term sea level curves based on plate tectonic models, generally do not incorporate detailed land-ice fluctuations resulting from the creation and destruction of ice sheets on multi-Myr scales. The works of Matthews et al. (2016), Müller et al. (2016), Seton et al. (2012) and Young et al. (2019), modelled eustasy using an ice-free world as starting point and therefore applied a static glacio-eustatic correction. Wright et al. 2020 applied a non-variable 70 m shift to their eustatic sea level curve. Karlsen et al. (2020) and Young et al. (2022), used and increasing correction going back into the Cenozoic of up to 57 m and 70 m respectively. Müller et al. (2018) incorporated the long-term fluctuations in global sea level during the last 38 million years from continental ice volume estimates from a zonally averaged energy balance climate model coupled to a one-dimensional ice sheet model (Stap et al., 2016a).

We here aim to produce a long-term eustatic sea level curve for the entire Phanerozoic that incorporates both changes in sea level driven by both plate tectonics as well as long-term glacio-eustacy. Our procedure uses the $^{87}Sr/^{86}Sr$ record from the oceans as a proxy for plate tectonic processes and combines it with a global estimate of the Cenozoic glacio-eustatic component of sea level (Bintanja and van de Wal, 2008; Stap et al., 2016b) and an estimate of Phanerozoic global temperature (Scotese et al., 2021). Importantly, this approach does not rely on information from local sedimentary basins or a detailed plate tectonic model of oceanic crust production through time, although can be compared with as such.

## 2. Methods

### 2.1. Sea level reconstruction from strontium isotope record

Strontium isotope ratios ($^{87}Sr/^{86}Sr$) record the combined input of strontium from mantle sources (mid-ocean ridge basalts & arc volcanism) and the weathering of continental radiogenic crust (Allègre et al., 2010). Van der Meer et al. (2017) quantified the mantle component of strontium by compensating the isotope data for the continental weathering component of the strontium cycle. This was obtained from climate modelling (Goddéris et al., 2014) linked to a surface weathering algorithm at 22 Phanerozoic and 7 Proterozoic time slices. Here weathering was assumed to be proportional to global run-off, which varied through geological time in this analysis. Using this procedure, van der Meer et al. (2017) estimated that variations in continental weathering could explain a maximum of ~20 % of the variation in the $^{87}Sr/^{86}Sr$ curve, whereas the remainder was related to the temporal variation in plate tectonic activity, i.e., subduction and correlated mid-ocean ridge spreading (van der Meer et al., 2017, 2014). Plume activity may account for additional variation on shorter time scales. For example, Large Igneous Provinces (LIPs) typically erupt over several million years. Events less than a few million years are not discernible in the strontium isotope record due to the longer residence time of Sr in the ocean (McArthur et al., 2012; Vollstaedt et al., 2014). Due to the limitations at short timescales (<few million years), the focus of our analyses is long-term eustatic sea level change.

The longer-term weathering of flood basalts has a second-order effect on the $^{87}Sr/^{86}Sr$ record, but current modelling (Mills et al., 2014) supports the conclusion that the strontium record is primarily driven by the production and subduction of oceanic crust through time (van der Meer et al., 2017). Preserved oceanic crust areas diminish with increasing age. For example, ocean crust younger than 50 Ma accounts for ~45 % of the modern ocean floor, while 30 % represents crust between 50 Ma and 100 Ma, and only the remainder (~25 %) is older than 100 Ma (Coltice et al., 2013; Seton et al., 2012; van der Meer et al., 2017). The modern age

versus area of oceanic crust can be described by a linear function (Parsons, 1982; Sclater et al., 1980; van der Meer et al., 2017). This area-age distribution of ocean floor is supported by plate tectonic modelling. Coltice et al. (2013) concluded that on model Earths with plate-like behaviour, the average area-age distribution is nearly linear, and that the average area-age of the ocean basins is directly correlated with the average spreading rates. Hence the $^{87}Sr/^{86}Sr$ ratio, after correcting for continental weathering, is primarily governed by the production of oceanic crust (Allègre et al., 2010; van der Meer et al., 2017), the $^{87}Sr/^{86}Sr$ record can serve as a proxy for the changing rates of global sea floor spreading (van der Meer et al., 2017). Using this approach, van der Meer et al. (2017) used the strontium isotope curve to estimate the production of oceanic crust as far back as 825 Ma (Neoproterozoic).

It was determined from the strontium isotope record that, compared to the present-day, plate tectonic activity (mid-ocean spreading, arc volcanism) was approximately twice as high from the mid-Jurassic to the late Cretaceous (170–80 Ma; van der Meer et al., 2017). These spreading rates are consistent with independent estimates from plate tectonic modelling (Spasojevic and Gurnis, 2012; Vérard et al., 2015) and estimates of Mesozoic plate activity derived from the record of ancient subducted slabs preserved in the mantle (van der Meer et al., 2018, 2014).

Oceanic crustal age is strongly correlated with the average depth of oceanic basement due to cooling of the oceanic lithosphere, increasing crustal thickness, and isostasy (Parsons and Sclater, 1977; Stein and Stein, 1992). Van der Meer et al. (2017), approximated the present-day relationship between the age of the ocean floor (Seton et al., 2012) and the corresponding depth of the ocean floor (Amante and Eakins, 2009) with a combined square root and linear function. The average depth of active ridges taken as constant, and increasing depth of the seabed the result of as an empirical relation of the combined effects of oceanic crust cooling, and secondary factors (Conrad, 2013; Müller et al., 2016; Simmons et al., 2020; Young et al., 2022) such as sedimentation, flood basalt deposition, dynamic topography. Pre-Cenozoic plate tectonic reconstructions of oceanic crustal age, however, are highly uncertain and this methodology has limited application for the Mesozoic and Paleozoic due to the lack of data and therefore high uncertainty (Müller et al., 2016; Torsvik et al., 2010).

As calculated from strontium isotope variability viewed over the Phanerozoic, not considering any climate effects, present-day eustatic sea level is very low due to a relatively low rate of mid-ocean-ridge spreading. This has been caused by the Cenozoic convergence and closure of smaller oceanic basins in the Tethys and Panthalassa Oceans (van der Meer et al., 2018, 2012) that led to a global decrease in subduction and mid ocean ridge spreading (van der Meer et al., 2017, 2014) and the establishment of large, long-lived oceans in the Pacific and Indo-Atlantic domains (i.e., Müller et al., 2008; Seton et al., 2012). In addition, but not quantified in our analyses, the area of the ocean basins may have increased due to the series of Cenozoic continental collisions that have reduced the area of continental lithosphere (Müller et al., 2008; Scotese and Wright, 2018). These continental collisions also increased the average elevation of the continents, hastening the retreat of the seas (Scotese and Wright, 2018). All of these plate tectonic factors have led to an average ocean crustal age of ~65 Ma, which is the oldest average age since the Jurassic (van der Meer et al., 2017; Williams et al., 2021). During Cretaceous time, average age of oceanic crust was ~30–40 Ma, leading to eustatic sea level being 150–300 m higher than present-day (Karlsen et al., 2020; van der Meer et al., 2017; Vérard et al., 2015; Williams et al., 2021; Wright et al., 2020). The long-term ~250 Myr periodicity or 'double-hump' in Phanerozoic eustatic sea level that is often reconstructed in eustatic sea level and continental flooding studies (Marcilly et al., 2022; Simmons et al., 2020), generally interpreted to be the result of supercontinent cyclicity (i.e. Nance and Murphy, 2019), was also observed in the $^{87}Sr/^{86}Sr$ based reconstruction of van der Meer et al. (2017). This consistency thereby suggests that at least for the long term (>50 Myr), the Sr-based method appears to be a suitable proxy for long term sea level reconstruction.

Since the publication of the $^{87}Sr/^{86}Sr$-based eustatic sea level reconstruction of Van der Meer et al. (2017), the $^{87}Sr/^{86}Sr$ record has been updated (McArthur et al., 2020) and new weathering estimates have become available. Initially, Van der Meer et al. (2017) chose to use the GEOCLIMtec climate-weathering model (Goddéris et al., 2014), available for 22 time-steps for the Phanerozoic, which included only the effects of changing paleogeography and solar flux – not changes to $CO_2$ degassing. In this study, we have now chosen to use the SCION model of Mills et al. (2021) which is based on the same climate reconstructions but includes variable degassing rates and can output run-off at one million year resolution, therefore providing more useful estimates of weathering for our purpose here. Although key inputs ($^{87}Sr/^{86}Sr$, weathering) have been updated, all other steps and calculations, summarized above, are the same as in Van der Meer et al. (2017).

The trends are very similar between the Van der Meer et al. (2017) estimate of eustatic sea level and the updated one presented in this study (Fig. 2). The few significant differences are higher eustatic sea level (~+50 m) in the late Cretaceous to Eocene and overall lower eustatic sea level in the Devonian-Carboniferous (~−50 m). Aside from the higher resolution of the SCION model, other changes from GEOCLIMtec include higher $CO_2$ levels for the Cenozoic and lower $CO_2$ levels in the Paleozoic, both of which are closer to proxy estimates (Foster et al., 2017; Mills et al., 2021). The elevated Cenozoic $CO_2$ degassing rates are derived from kinematic models rather than the ridge volume estimates. $CO_2$ levels are lower for the Paleozoic because SCION includes erosion in its weathering calculation (Mills et al., 2021), whereas the older version of GEOCLIM did not. The uncertainty in global runoff (Fig. 2A) is derived from an ensemble of model runs where the degassing rates are varied between different recent estimates (Brune et al., 2017; Domeier and Torsvik, 2017; Mills et al., 2019) and the contribution of land plants to amplifying weathering rates is varied between no change and a 7-fold increase (e.g. Berner, 1991; Lenton, 2001). Other sources of uncertainty, not quantified here, are other global processes that have uncertainty and will impact the $CO_2$ level, such as continental lithology or organic carbon cycle imbalance. But these have not yet been worked into the model in a way that would allow uncertainty testing.

### 2.2. Paleotemperature reconstruction

The total mass of water stored in continental ice sheets can be estimated, although imperfectly, using an oxygen isotope ratio ($\delta^{18}O$) mass balance (Shackleton, 1967). Ice sheets are depleted in the $^{18}O$ isotope relative to $^{16}O$, which means oceans are $^{18}O$-enriched during the expansion of continental ice sheets. Variations in continental ice volume can thus be assessed through reconstructions of seawater $\delta^{18}O$ as recorded in deep sea benthic foraminifera (e.g., (Hays et al., 1976; Shackleton and Opdyke, 1973). This approach is however complicated by the fact that foraminiferal $\delta^{18}O$ is also affected by ocean temperature (Shackleton et al., 1973), therefore, a temperature component must be subtracted, for example using Mg/Ca ratios (Lear et al., 2000). It has also been noted that the $\delta^{18}O$ composition of ice sheets varies through time (e.g., (DeConto et al., 2008).

For the Late Cenozoic, several comprehensive analyses have been carried out to calibrate $\delta^{18}O$ with eustatic sea level. The use of the $\delta^{18}O$ isotope record has been employed to correlate stratigraphic sea level curves with the reconstructed ice volume and

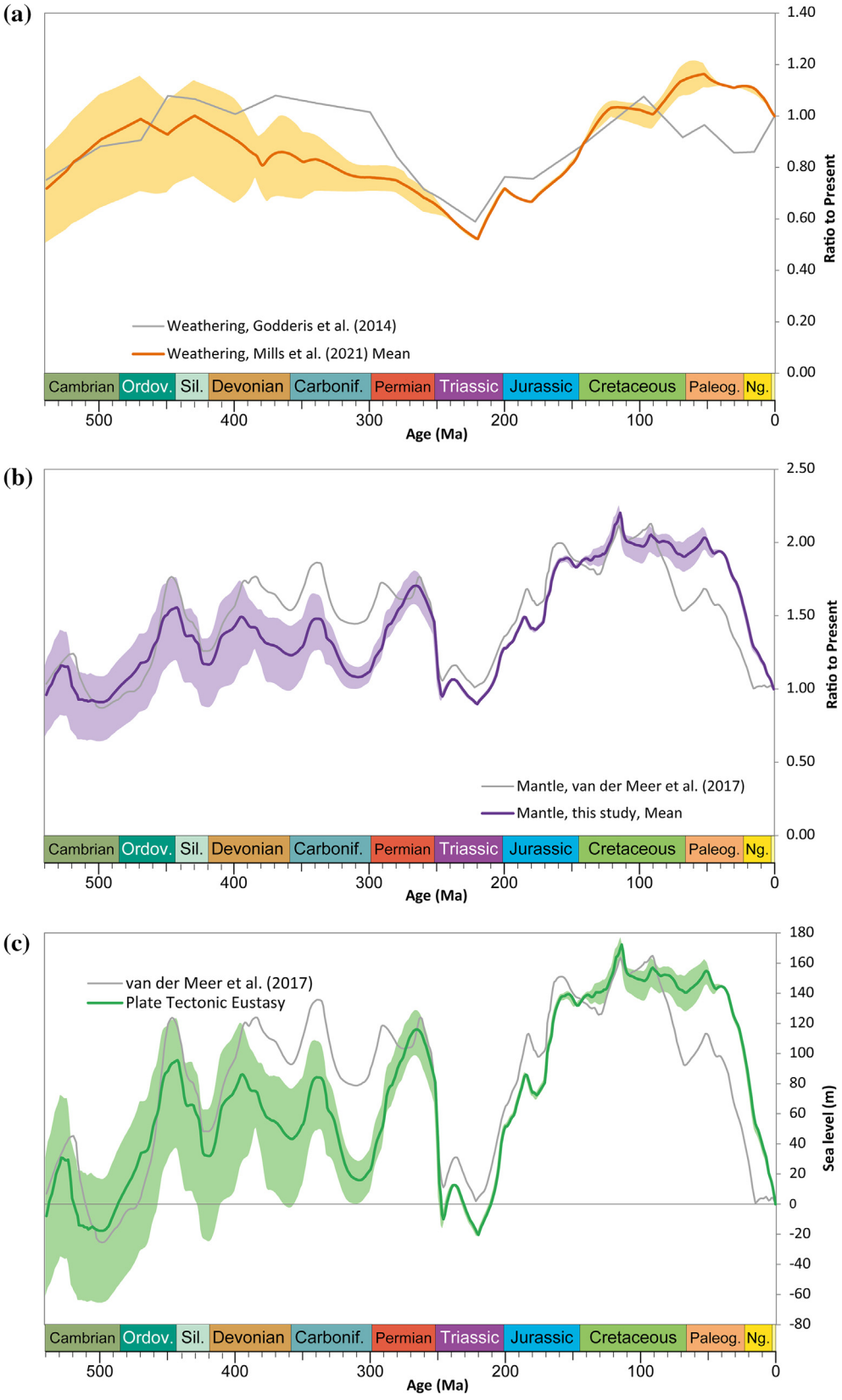


**Fig. 2. Plate tectonic eustasy from $^{87}Sr/^{86}Sr$.** Forcings of $^{87}Sr/^{86}Sr$ from **a)** weathering component (black line) and uncertainty ranges (shaded orange) from Mills et al. (2021), with a comparison with the previously used estimates from Goddéris et al. (2014) (grey line) **b)** mantle component (plate tectonic) forcing and uncertainty ranges (shaded purple), calculated using methodology of van der Meer et al. (2017), using the weathering inputs of Mills et al. (2021) **c)** Plate tectonic eustasy using the methodology of van der Meer et al. (2017) with updated $^{87}Sr/^{86}Sr$ inputs from McArthur et al. (2020) and weathering inputs from Mills et al. (2021). Uncertainty ranges (shaded green) result from the propagation of weathering uncertainties (Fig. 8). For comparison the older analyses of van der Meer et al. (2017) are shown in b) and c) (grey line). Results available in Supplementary Table 1.

hence changes to overall seawater volume (Browning et al., 1996). Most recently, Miller et al. (2020) used deep ocean benthic foraminiferal $\delta^{18}O$ records, combined with stratigraphic analyses of the New Jersey shelf (Kominz et al., 2016; Miller et al., 2005) to reconstruct global mean sea level. Although this is likely the best stratigraphically derived eustatic sea level reconstruction (but still subject to the overall interpretation ambiguity from stratigraphic methods) it is limited to the Cenozoic.

Bintanja and van de Wal (2008), De Boer et al. (2010) and Stap et al. (2014) used benthic foraminifera $\delta^{18}O$ to evaluate the relationship between temperature, eustatic sea level, and the volume of continental ice sheets. They compared the $\delta^{18}O$ records for the past 0.8 Myr with a high-frequency record of sedimentation in the Red Sea (Rohling et al., 2009) and coral reef data from New Guinea and the Barbados (Lambeck and Chappell, 2001). Although these Pleistocene studies provide some background on constraints regarding changing eustatic sea level in more recent times, the goal of this study is to describe longer-term forcing. Stap et al. (2017) estimate the water volume sequestered in Northern Hemisphere and Antarctic icecaps since the inception of the Antarctic icecap at the Eocene-Oligocene transition (~34 Ma). Their estimate of eustatic sea level variation, however, is simply a land ice-volume-equivalent, using a fixed marine area, and does not consider flooding of the continental shelf.

Few studies exist that attempt to reconstruct eustatic sea level based on $\delta^{18}O$ before the formation of the Antarctic ice cap (~34 Ma). Miller et al. (2005) matched $\delta^{18}O$ variations with stratigraphically derived sea level estimates, but did not consider plate tectonic, ice volume, or steric effects. In other stratigraphically derived curves, qualitative comparisons to $\delta^{18}O$ have been made, (Abreu et al., 1998; Haq, 2018a; Miller et al., 2005), but no quantitative reconstructions of sea level from $\delta^{18}O$ have been attempted.

Another concern is the possibility that the $\delta^{18}O$ composition of the global exogenic water pool (notably the sum of oceans and ice sheets) has changed over time, although reconstructions suggest this was not a major factor over the past 100 million years (de Bar et al., 2019). However, if we assume that the $\delta^{18}O$ composition of sea water has been constant throughout the Phanerozoic, then $\delta^{18}O$ measurements of tropical temperatures from early Paleozoic fossils would require Sea Surface Temperatures (SST) in excess of 40 °C (i.e. Song et al., 2019). Such high temperatures would challenge biotic tolerances (Frieling et al., 2017; Sherwood and Huber, 2010). Various studies have attempted to resolve this high temperature anomaly by "detrending" the $\delta^{18}O$ curve with exponential (Veizer and Prokoph, 2015) or linear (Vérard and Veizer, 2019) adjustments. The constancy of $\delta^{18}O$ in seawater remains controversial. It seems that over long periods of time (>100 Myr) the $\delta^{18}O$ composition of seawater may change, whereas the $\delta^{18}O$ composition of seawater over shorter time intervals (10's of millions of years) may be relatively stable and thus may be used to estimate paleotemperatures.

Global Climate Model (GCM) simulations are another way of reconstructing Phanerozoic temperature estimates. However, they have limitations: Firstly, they do not have the temporal resolution provided by the combined geological & geochemical data sets. Secondly, the principal way GCMs modulate temperature is by varying the amount of $CO_2$. However, each model reacts differently to $CO_2$ and the Phanerozoic record of $CO_2$ still has large gaps. As an example Valdes et al., 2021 (Fig. 3) constrains deep ocean temperatures with $\delta^{18}O$ from benthic foraminifera and the modelling works well and prior to the Cretaceous deep ocean temperatures would probably be an unreliable indicator of global mean surface conditions.

Although GCMs are constantly improving their rendition of deep time climates, we are confident that the geological record combined with geochemical proxy information of Scotese et al. (2021) provide a more detailed and accurate measure of changing global temperatures during the Phanerozoic.

Scotese et al. (2021) combined temperature changes on three different time scales. At the longest timescale (~100 Myr), lithologic indicators of climate such as evaporites, bauxites, and tillites were used to reconstruct paleo-Köppen belts and the pole-to-equator temperature gradient. Although each climate indicator carries uncertainty on temperature conditions, this combined record is the best available to science. These estimates of global average temperature were used to reconstruct long-term paleotemperature trends. At medium term timescales of 10 to 20 million years, $\delta^{18}O$ paleotemperature proxies (Song et al., 2019) were used to reconstruct medium-term temperature trends. On the shortest

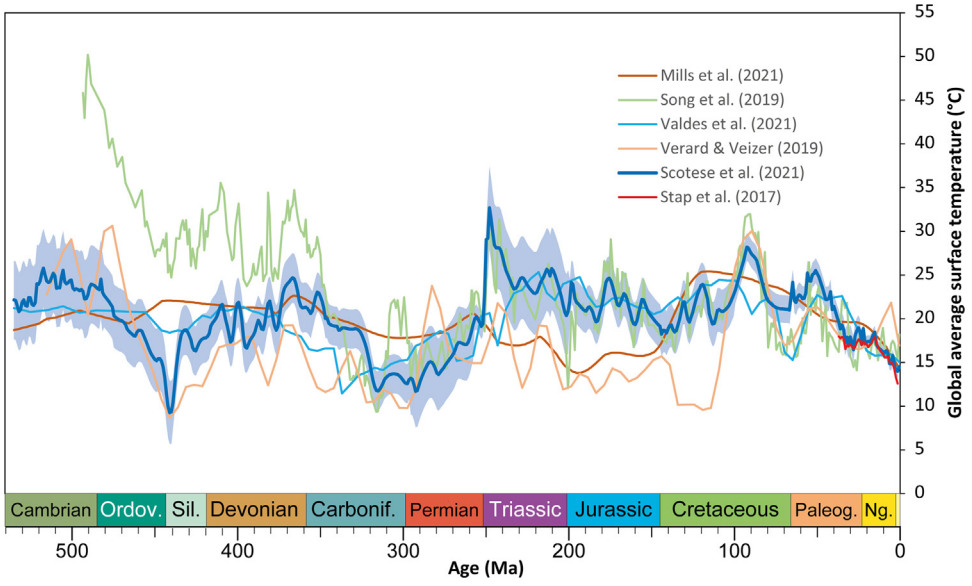


**Fig. 3. Global average surface sea level temperature.** We use the most recent paleo-temperature reconstruction of Scotese et al. (2021), in combination with the coupled ice-sea level-climate model of Stap et al. (2017) for the Cenozoic. RMS uncertainty ranges (shaded blue), calculated from $\delta^{18}O$ and paleo-Köppen zone uncertainties, of Scotese et al. (2021). Results available in Supplementary Table 1. Other curves based on $\delta^{18}O$ (Song et al., 2019; Vérard and Veizer, 2019) and climate models (Mills et al., 2021; Valdes et al., 2021) are shown for comparison.

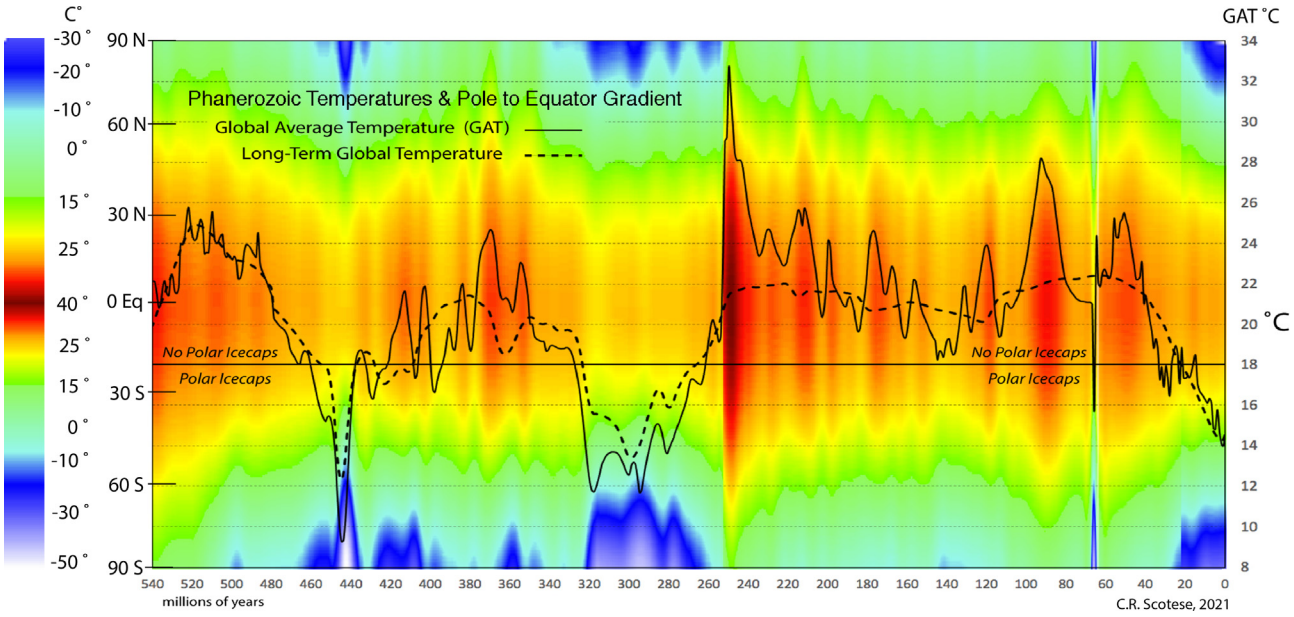


**Fig. 4. Phanerozoic temperatures and pole-to-equator temperature gradients**. Data from recent paleo-temperature reconstruction for the Phanerozoic (Scotese et al. 2021).

term (up to a few Myr), potential effects of flood basalt related degassing and cooling effects of bolide impact winters were noted. This model of Phanerozoic paleotemperatures (Scotese et al., 2021) is one of most recent comprehensive reconstructions of Earth's global paleotemperature history and we therefore use it to estimate the timing and amount of continental ice during the Phanerozoic. The only correction we have made is to remove the Cretaceous-Paleogene downward temperature spike, as inferred from the Chixculub bolide impact winter. Bolide impact winters last only years to decades at most (Vellekoop et al., 2014, 2016), insufficient to lead to impact ice volume and eustatic sea level. In addition, there are no indications that ice caps may have formed in this short time interval.

The Scotese et al. (2021) Phanerozoic paleotemperature curve is shown in Fig. 3. For comparison we also show the paleotemperature curves of (Mills et al., 2021; Song et al., 2019; Vérard and Veizer, 2019). Generally, the three curves have similar trends between 0 and 110 Ma, but significant differences exist before 110 Ma. The pre-350 Ma temperatures of Song et al. (2019) assume a constant $\delta^{18}O$ composition of seawater and appear to be much too high given likely biological tolerances. Vérard and Veizer (2019) attempted to correct this anomaly by applying a linear correction that decreased the $\delta^{18}O$ of seawater back in time. While this correction works for the last 100 million years, it appears to 'overcorrect' for older time intervals. The resulting cooler global temperatures predict extensive glacial ice-caps in the early Mesozoic and the Siluro-Devonian, however, there is no evidence of glacial deposits from polar ice caps at these times (Boucot et al., 2013; Cao et al., 2019). In comparison, the curves of Mills et al. (2021) and Song et al. (2019) have not made a correction of $\delta^{18}O$, and Scotese et al. (2021) applied a non-linear correction, tied to paleo-Köppen zones as described above. As such, these studies have generally higher temperatures than Vérard and Veizer (2019), except for intervals known to have extensive ice sheets.

### 2.3. Perennial ice paleolatitude reconstruction

Using the Phanerozoic paleotemperature model of Scotese et al. (2021), we can estimate the past latitude of the polar ice front. The classic Budyko-Sellers energy balance models (Budyko, 1969; Caldeira and Kasting, 1992; Sellers, 1969) assume that snow and ice will be present year-round at a particular latitude when the annual average temperature is less than −10 °C. This agrees well with the observation that the average latitude of the modern permanent snowline in the northern hemisphere (i.e., tundra) is 67 °N, which corresponds with an average annual temperature of −9.5 °C.

Using an annual average temperature of −10 °C, as explained above, to define the polar ice limit, the latitude at which this temperature occurred was recorded from 120 pole-to-equator gradient plots that described changing Phanerozoic paleoclimates. (Scotese et al., 2021; Supplementary Materials). For example, during the Middle Miocene Climatic Optimum (15 Ma), the −10 °C isotherm occurred at a latitude of 78° in the northern hemisphere and a latitude of 72° in the southern hemisphere (Fig. 4). In contrast, the Permo-Carboniferous Glacial Maximum (295 Ma), the −10 °C isotherm occurred at a latitude of 68° in the northern hemisphere and a latitude of 56° in the southern hemisphere (Fig. 4). Similar measurements were made for the complete set of pole-to-equator diagrams derived from the Scotese et al. (2021) Phanerozoic paleotemperature model.

Scotese et al. 2021 did not publish uncertainty ranges for their paleo-temperature reconstruction. In an attempt to quantify these, we estimate the uncertainty ranges of Scotese et al. (2021) by calculating the Root-Mean-Squares uncertainty of the temperature reconstruction from $\delta^{18}O$ data of Song et al. (2019) and an estimate of the Köppen-zone uncertainty range, based on the number of sample localities (Boucot et al., 2013; Scotese et al., 2021). The uncertainty ranges are summarized in Table 1 and shown in Fig. 3. Due to the high variability in $\delta^{18}O$ data for every 1 Myr (Song et al. 2019), our uncertainty estimation is appropriate for trends over > 5 Myr timescales, the focus of our analyses. We have tested the extreme ends of the RMS temperature uncertainty ranges and found that temperatures beyond these ranges would lead to irreconcilable differences with the geological climatological data (Boucot et al. 2013, Scotese et al. 2021).

As seen from Fig. 5, the ice front temperature changes as the global average temperature changes. Despite the somewhat different curvatures and hemispherical asymmetries in the pole-to-equator temperature plots of Scotese et al. (2021), there is a clear linear relationship between the latitude of the polar ice front and

**Table 1**
**Uncertainty propagation of paleo-temperature reconstruction.** Temperature uncertainties summarized from Song et al. (2019). Paleo-Köppen-zone uncertainty estimated from Scotese et al. (2021). The Root-Mean-Square (RMS) temperature uncertainty is used further in our analyses.

| Epoch Interval | Age Interval (Ma) | Temperature Uncertainty (°C) | Paleo-Köppen-zone Uncertainty (°C) | RMS Uncertainty (°C) |
|---|---|---|---|---|
| **Neogene** | 0–23 | 0.5 | 0.5 | 0.7 |
| **Paleogene** | 24–65 | 1 | 1 | 1.4 |
| **Late Cretaceous** | 66–100 | 0.5 | 1.5 | 1.6 |
| **Early Cretaceous-Jurassic** | 101–201 | 2 | 1.5 | 2.5 |
| **Triassic** | 202–251 | 4 | 2.5 | 4.7 |
| **Lopingian** | 252–259 | 1 | 1 | 1.4 |
| **Guadalupian-Cisuralian** | 260–298 | 4 | 1 | 4.1 |
| **Carboniferous** | 299–358 | 2 | 1 | 2.2 |
| **Devonian-Silurian** | 359–443 | 2 | 2 | 2.8 |
| **Ordovician** | 444–485 | 2 | 3 | 3.6 |
| **Cambrian** | 486–541 | 2 | 4 | 4.5 |

average annual temperature. This relationship is given in Equation 1, which we will use for further calculations.

For the late Cenozoic (0–20 Ma) time intervals, when both hemispheres reach temperatures less than −10 °C, the following relationship is observed, which we will use going forward:

$$\text{Latitude of the Polar Ice Front } (\circ) = 2.3356 * \text{Annual Average Temperature } (\circ C) + 31.818. \quad (1)$$

In comparison, for all of the Phanerozoic data points with larger uncertainty ranges, a less certain but similar relationship is observed:

$$\text{Latitude of the Polar Ice Front } (\circ) = 2.4568 * \text{Annual Average Temperature } (\circ C) + 33.127. \quad (2)$$

We note that our empirical trend is different from the curve used in Mills et al. 2019, which was also derived from Cenozoic ice area – temperature relationships (Hansen et al., 2013). The difference is because Mills et al. (2019) took the last glacial maximum rather than the current interglacial to represent present-day. They also used an older paleolatitude reconstruction of the glaciation record (Crowley and Burke, 1998).

Solving the equations for the modern annual average temperature (14.5 °C), we obtain an estimate of the present-day polar ice front of 69.7° (Equation 1), and an estimate of 67.8° using Equation 2. Both estimates of the permanent ice cap are close to the observed latitude of the permanent ice caps (67° N and; 66.5° S). For the coldest times during the Phanerozoic, this model predicts that the polar ice front may have expanded equatorward to latitudes of 55–60° N & S (Fig. 6). Conversely, during hot house intervals, when annual global average temperatures exceeded 20 °C, permanent ice would only have been found within a few 100 kms of the poles (Fig. 6).

The predictions derived from the Scotese et al. (2021) temperature model regarding the paleolatitude of the polar ice front can be tested by plotting the known paleolatitude of glacial deposits (Fig. 6). We compare our paleolatitude of polar ice front, with the tillites

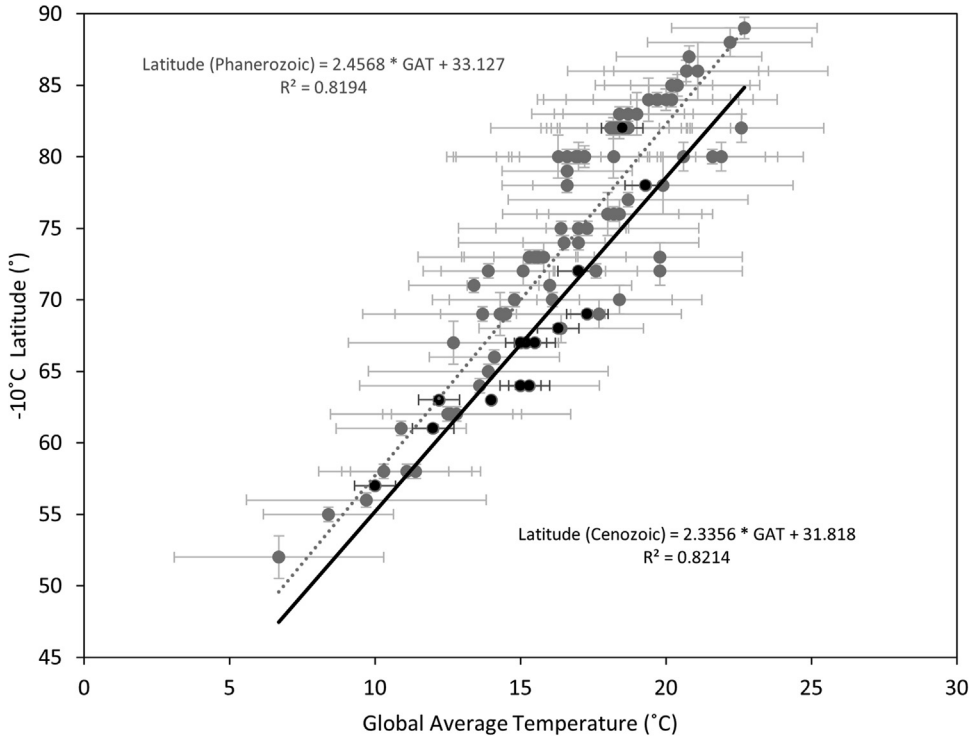


**Fig. 5. Paleolatitude estimation of the Polar Ice Front as a function of Annual Average Temperature.** Each data point records the paleolatitude of the −10 °C isotherm derived from the pole-to-equator plots of Scotese et al. (2021). The black dots represent late Cenozoic (0–20 Ma) data points with a solid trendline. The grey dots represent all Phanerozoic data points, dotted trendline, for comparison. Temperature uncertainty estimates in Table 1. −10 °C Latitude uncertainty estimates estimated to be 50 % of paleo-Köppen zone-uncertainty ranges.

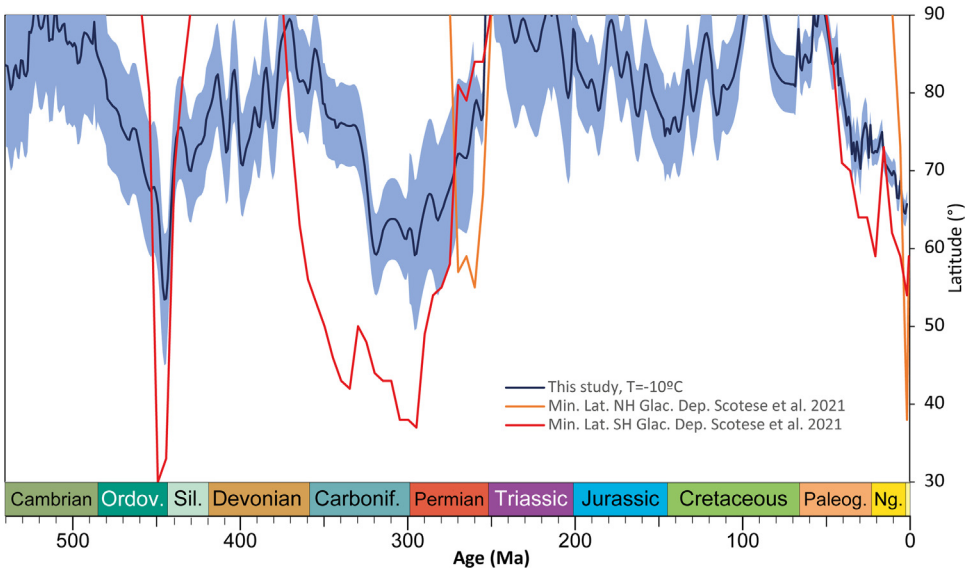


**Fig. 6. Paleolatitude of the polar ice front during the Phanerozoic.** Our estimate is based on average temperature less than −10 °C, used as a defined threshold for perennial ice sheet formation. Uncertainty ranges (shaded blue) were calculated by using Equation 1, and the Global Average Temperature uncertainty (Fig. 4). Results available in Supplementary Table 1. For comparison we minimum latitude of mapped glacial deposits on southern and northern hemispheres (Scotese, 2021; Scotese et al., 2021) are also shown.

distribution of Boucot et al. (2013), but not glendonites and dropstones as these are not indicators of continental ice caps. These tillites were used to derive polar ice extents in the Supplemental Material of Scotese et al., (2021), a recent summary of paleogeography (Scotese, 2021) and have also been used in paleo-climate simulations (Valdes et al., 2021). These ice extents were estimated on paleogeographic maps for every 5 million years. As such they are an update of the Cao et al., (2019) study, which were based on maps for every ~20 million years and did not include the Cambrian-Ordovician.

It should be noted that the minimum latitude of tillites is not directly comparable with our paleo-latitude perennial ice reconstruction. The minimum latitude of tillites can be from a relatively confined location at short time interval (<1 Myr), and therefore not representative of a global average, at Myr timescales. For example, Pleistocene ice sheets reached the Ohio River (37°N), however the "average" latitude was ~57°N. As such the minimum latitude of tillites, is not representative for the presumed area of continental ice and may lead to overestimation. As seen in Fig. 6, at peak icehouse times (Cenozoic, Permo-Carboniferous, Ordovician), the minimum latitude of tillites exceeds our perennial ice latitudes.

During other times, the temperature-based estimates of small continental ice sheets during the middle Paleozoic and Jurassic-Cretaceous may explain some of the eustatic fluctuations discussed later - even though no tillite deposits are described in Boucot et al. (2013). Potentially these are not preserved, or not included in their database. For example, tillites of Valanginian-Aptian age have been described in Australia (Alley and Frakes, 2003) but are not included in the database of Boucot et al. (2013), and as such no permanent ice sheets have been included in recent paleogeographic maps (Scotese, 2021; Scotese and Wright, 2018).

There are also several reasons why the temperature model might lead to an inaccurate perennial ice prediction. Firstly, zonal temperature differences exist even within one ocean basin, as also reconstructed in the paleo-domain (e.g. Douglas et al., 2014). Secondly, high latitude temperature reconstructions do not correspond very well to deep ocean temperatures for the Cenozoic (Cramwinckel et al., 2018). Thirdly, ice sheets are associated with significant hysteresis (growth and melt do not occur close to the same boundary conditions) (e.g. DeConto and Pollard, 2003). Most importantly ice sheets create their own elevation and so as soon as there is a 1 km thick ice sheet, temperatures on its surface are ~7 °C lower only due to lapse rate. Fourthly, there are wet-based (Greenland) and cold-based (Antarctica) ice sheets and their relation to temperature is very different as they have a very different hydrological basis (e.g. DeConto et al., 2008). In other words, their formation and melting thresholds are different. Fifthly, mean annual temperature is not a determining factor in ice sheets; they dominantly respond to snowfall and summer temperature (Hays et al., 1976; Milanković, 1941). Some of these factors may be irrelevant on the time scales we are investigating (>1 Myr), but we will address potential overestimating/underestimating effects in the discussion. With all the caveats listed above, our derived temperature threshold should be considered as a rough proxy for perennial ice formation.

### 2.4. Land and shelf ice areas estimation

The paleolatitude of the polar ice front was used to estimate the area of continental ice cover (Fig. 7). The continental area at high latitudes is based on the digital paleogeographic maps of Scotese and Wright (2018) and Scotese (2021). We utilized these paleo-digital elevation models, to separate land ice (above sea level), grounded ice on shelf margins (continental crust, defined at −1000 m isobath), and sea-ice (Fig. 7). Our analyses have similar trends to Scotese's mapped ice extent, notably for the well-constrained Cenozoic land ice. There is less correlation in amplitude for the more poorly constrained shelf ice and in the Paleozoic ice ages.

The bulk of stored water in ice sheets is on land, to a lesser extent on grounded ice on shelf margins (decreasing with water depths), whereas floating sea ice does not store any water out of isostatic equilibrium. Using the same cut-off points as Scotese et al., we calculate the theoretical perennial ice extent on land, and on shelf margins (using −1000 m isobath). We ignore any potential grounded ice shelfs on water depths greater than 1000 m. Although thick (>1100 m) ice sheets may still get grounded there, a detailed analyses of the Scotese and Wright (2018) digital elevation model shows that there is a progressively decreasing (ice-prone high-latitude) area added for every 100 m depth interval

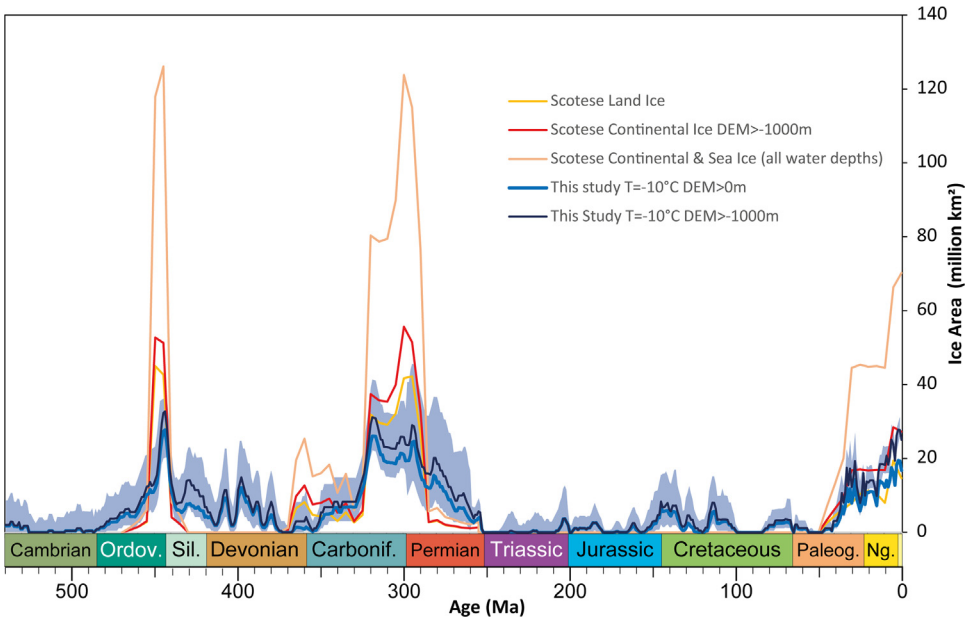


**Fig. 7. Perennial ice area estimates.** Our estimates are based on the paleo-latitude of the polar ice front and correlation with land (DEM > 0 m) and shelf margin (DEM > −1000 m) at equivalent and higher latitudes The propagation of polar ice front paleolatitude uncertainty (Fig. 6) results in ice area uncertainty (shaded blue). Results available in Supplementary Table 1. For comparison we show mapped ice areas on land, continental crust and sea (Scotese, 2021; Scotese and Wright, 2018).

beyond the globally averaged shelf-slope break (~200 m). Therefore, we consider any area additions beyond −1000 m to be insignificant.

### 2.5. Estimating the volume of water stored in continental ice sheets

To estimate the amount of water stored in continental ice sheets, we separate ice stored on land and the 'net' ice stored in ice sheets grounded on the seabed. We correlate the total 'net' ice with a coupled ice sheet climate model, which calculated internally consistent estimates of temperature, ice volume, sea level, and $pCO_2$ from the oxygen isotope records of deep sea benthic foraminifera (0–38 Ma; Stap et al., 2017). Stap et al. (2017) derived their ice volume equivalent (unspecified whether on land, or net effect of grounded ice on shelf) from sea level calibrated with a 120 m sea level drop during the Last Glacial Maximum (de Boer et al., 2010; Stap et al., 2014).

Land ice conversion to water is straightforward, and merely involves multiplication with the relative density difference (0.91 De Boer et al. 2010). For the grounded ice sheets on the shelf, in excess of the isostatic equilibrium, we approximate the stored water volume as follows. We multiply the area of the ice-covered shelf with the height of the ice sheet minus the isostatic equilibrium height and linearly averaged water depth of 500 m.

Using the generalized reduced gradient method, we calculate a best-fit total ice-thickness for the 1–37 Ma interval (Fig. 8) of Stap et al. 2017. As can be seen in the figure we obtain a good trend match between the results of Stap et al. and ours. Our best fit is a 1.4 km average ice sheet thickness, with 1.1 and 1.8 km thickness as lower and upper bounds respectively for the Cenozoic temperature uncertainty ranges. The Present-day polar ice thickness (1.9 km), as calculated from a recent topographic model (Hirt and Rexer, 2015) falls outside this range, but it is not representative for the average over 1 Myr time intervals. During periods of short term ($\ll$1 Myr) glacial periods, ice thicknesses are expected to have been larger than the 1 Myr average. Using the average thickness, we then calculated the volume of ice for the Phanerozoic (Fig. 8). The volume of net ice ranged from a few million km$^3$ during Mesozoic "cold snaps" to up to 40–60 million km$^3$ of continental ice during the late Ordovician, Permo-Carboniferous, and Neogene icehouse intervals.

Using the calibration with Stap et al. (37–1 Ma), there is logically only relatively small uncertainty ranges remaining in our ice volume calculations at individual time steps in the Cenozoic. Larger uncertainties are present in the Mesozoic and Paleozoic, reaching up to 25 million km$^3$.

### 2.6. Glacio-eustatic sea level change

Given the volume of net continental ice through time (Fig. 8), we calculated the changes in eustatic sea level due to the waxing and waning of the continental ice sheets (at 1 Myr intervals). In this calculation we assumed: a constant volume of water, a variable average depth of the ocean floor (using $^{87}Sr/^{86}Sr$), and a constant hypsometry of the continental shelf (van der Meer et al., 2017).

As shown in Fig. 9, the resulting maximum long-term absolute glacio-eustasy ranges from 60 m above present-day sea level to 30 m below sea level (isostatically compensated).

We re-distribute the water over the oceans and continental shelf areas, using the linearly approximated shelf hypsometry, and variable ocean floor depth, as described in van der Meer et al. (2017). The resulting new Tectono-Glacio-Eustatic curve is shown in Fig. 10.

## 3. Results and discussion

The combined effect of plate tectonics (<190 m), and glacio-eustasy (<90 m) produced a combined amplitude in eustatic sea level of up to ~220 m during the Phanerozoic (Figs. 10, 11). Describing the most significant amplitude extremes we note that the Cretaceous has the highest eustatic sea level (174–217 m) of all Periods, with peaks in the Aptian (217 m; 117 Ma) and Turonian (211 m; 91 Ma). Other notable highstands of eustatic sea level occurred during the early Eocene (209 m; 51 Ma), late Jurassic (194 m; 155 Ma), late Permian (152 m; 268–260 Ma), Mississip-

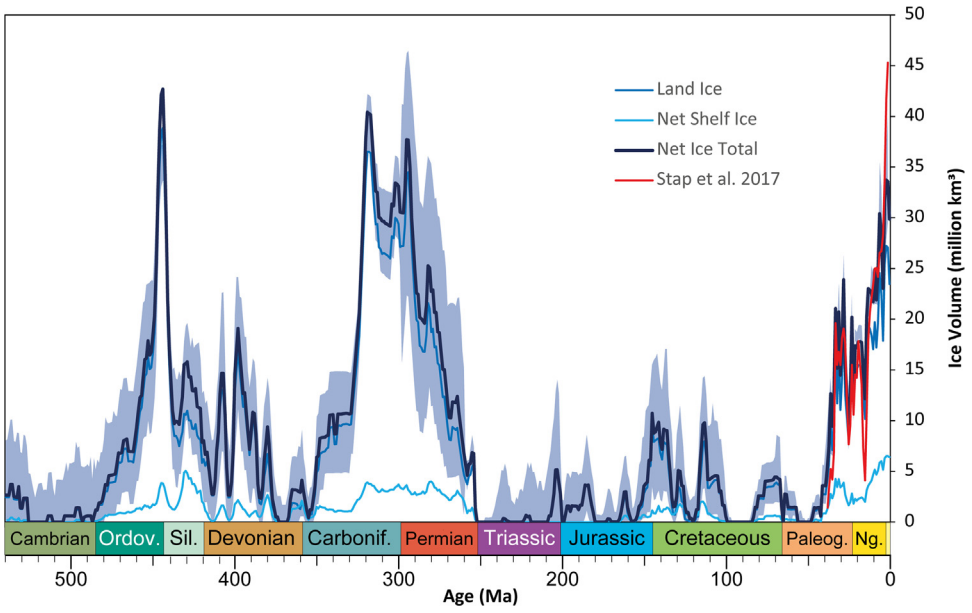


**Fig. 8. Perennial ice volume estimates.** Net ice volume from land, grounded ice sheets on shelf margins, and total net ice using T = −10 °C, DEM cut-offs at 0 m and −1000 m, with linearly averaged water depth of 500 m. Uncertainty ranges (shaded blue) result from the propagation of ice area (Fig. 7) & thickness uncertainty range, calibrated to Stap et al. (2017) in the late Cenozoic. Results available in Supplementary Table 1.

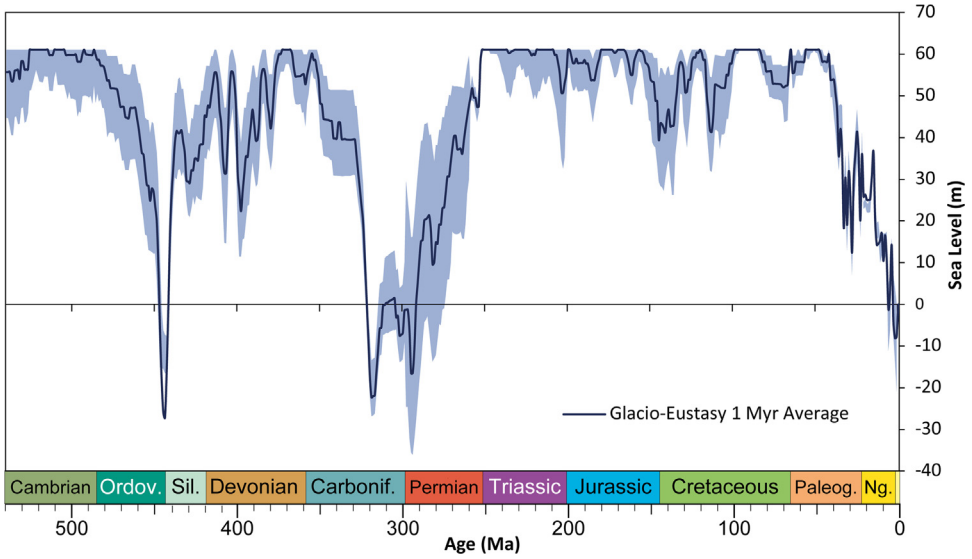


**Fig. 9. Glacio-eustasy.** Isostatically compensated effects of glacio-eustasy for the Phanerozoic (1 Myr time steps), assuming a constant ocean-floor depth. Uncertainty ranges (shaded blue) result from the propagation of ice volume uncertainties (Fig. 8). Results available in Supplementary Table 1.

pian (125 m; 338 Ma), and middle Devonian (128 m; 385 Ma). Eustatic sea level was lowest during the icehouse worlds of the latest Cenozoic (<10 Ma) and Permo-Carboniferous (320–295 Ma); Notable falls in eustatic sea level also occurred during the Hirnantian Ice Age (445 Ma) and during the late Permian, Triassic and early Jurassic (250–200 Ma).

In the following section, we describe Phanerozoic eustatic sea level in terms of long-term (>50 million years), and the residual medium (10 to 20 million years) sea level changes.

### *3.1. Long-term eustatic sea level trends (>50 Myr)*

Long-term eustatic sea level trends (>50 Myr) are primarily driven by the plate tectonic cycle (Cloetingh and Haq, 2015; Conrad, 2013; Ray et al., 2019; van der Meer et al., 2017) and we calculate plate tectonic eustasic changes of up to 190 m (Fig. 10). The 'double-hump' supercontinent cycle is still recognizable in the Tectono-Glacio-Eustatic curve, with a high in the Cretaceous-Eocene and pronounced troughs in the Triassic and late Cenozoic (Fig. 11). For the Cretaceous-Cenozoic, amplitude and long term trends are qualitatively similar to stratigraphic derived Haq et al. compilation, continental flooding (Marcilly et al., 2022), and most plate tectonic modelling studies (Karlsen et al., 2020; Vérard et al., 2015; Wright et al., 2020), with the exception of Young et al. (2022). Differences become greater further back in time.

Some plate tectonic modelling derived eustatic sea level curves (Fig. 11) have a more pronounced Paleozoic long-term high (Karlsen et al., 2020; Young et al., 2022). Higher amounts of ridge

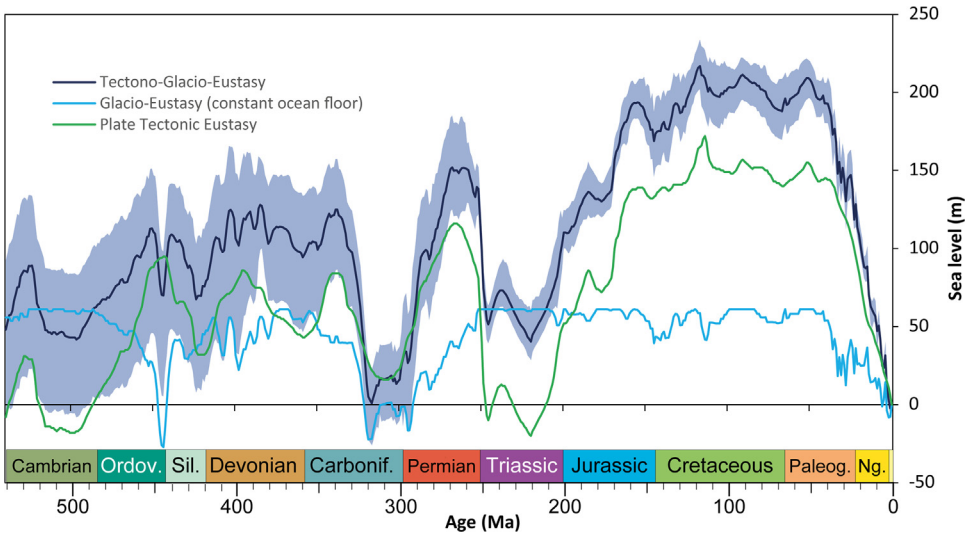


**Fig. 10. Eustatic components.** Isostatically compensated effects of plate tectonics (strontium record, green), net ice (turquoise) and our combined Tectono-Glacio-Eustatic curve (blue) including RMS uncertainty ranges (shaded blue), calculated from the uncertainties in plate tectonic eustasy (Fig. 2C) and Glacio-eustasy (Fig. 9). Results available in Supplementary Table 1.

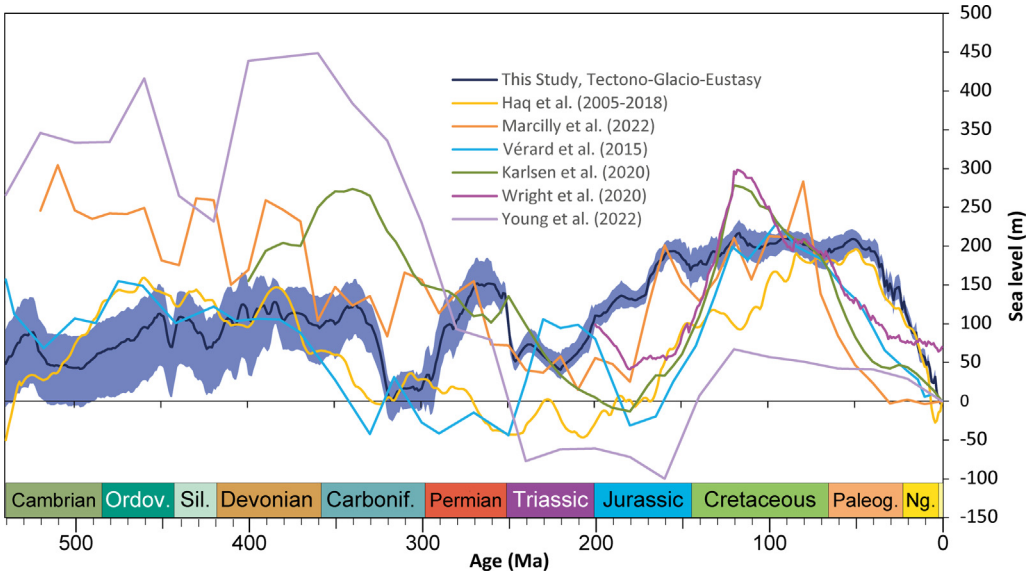


**Fig. 11. Phanerozoic eustatic sea level curves.** Our Tectono-Glacio-Eustatic curve shown in comparison with curves resulting from plate tectonic modelling, continental flooding, and a compilation derived from stratigraphy.

spreading in the underlying plate model, leading to large areas with shallow young oceanic lithosphere (Karlsen et al., 2020; Matthews et al., 2016) seem to be the main cause, in addition to assumed water flux into the mantle (Young et al., 2022). There are smaller differences with the plate tectonic modelling reconstruction of Vérard et al. (2015). However, due to the absence of preserved oceanic crust, all plate modelling reconstructions are entirely model driven before the Jurassic, hence any difference or agreement could be coincidental. Likewise, there is agreement with the overall amplitude and general trend of the Paleozoic highstand of Haq and Al-Qahtani (2005), but given the flaws of the stratigraphic method, this could be entirely coincidental. Lastly the continental flooding derived sea level curve of Marcilly et al. (2022), has limited agreement in the Paleozoic, which may be related due to continental destruction or growth, which has not been incorporated by our analyses. Clearly more work is required to understand the differences and future improvements of either methodology.

Our calculated quantitative effect of land ice in the Cenozoic (~60 m) is within the range suggested by previous studies: 54 m (Müller et al., 2008), 57 m (Conrad, 2013) and more recently 70 m (Wright et al., 2020; Young et al., 2022). The combined effect of plate tectonics and glacio-eustasy cause a drop in eustatic sea level of > 200 m during the last 50 Myr. Although amplitudes vary, falling sea level since the mid-Eocene has been uniformly recognized in numerous stratigraphic studies (Haq et al., 1987; Kominz et al., 2008; Miller et al., 2020; Vail et al, 1977).

The late Paleozoic icehouse is most important regarding long-term eustatic sea level change, with an overall glacio-eustatic effects of up to < 90 m within a 105 Myr interval between ~355–250 Ma (Figs. 7, 8 & 9). Ice sheet formation is supported by geological evidence of glacial deposits (Boucot et al., 2013; Cao et al., 2019) and as a result large land-based ice sheets have been inferred (Scotese, 2021; Scotese and Wright, 2018). In our analyses, the combined tectonic and glacio-eustatic effect (Fig. 10) reaches up to 150 m (at > 1 Myr time scales) in the late Paleo-

zoic. The large amplitude (>100 m) fits well with stratigraphic studies (Rygel et al., 2008; Saunders and Ramsbottom, 1986), although the cause is generally attributed purely to glacio-eustacy, and not partly to tectonics. A major eustatic event occurred at the mid-Carboniferous and the Mississippian-Pennsylvanian unconformity in North America is often cited as evidence for the initiation of the large south polar ice sheet on Gondwana. Equally prominent are contemporaneous unconformity surfaces are also present in Europe, North Africa, and elsewhere (Saunders and Ramsbottom, 1986).

When we compare our eustatic sea level curve, which incorporates ice volume effects, with the sea level curve derived solely from plate tectonic effects predicted by changing $^{87}Sr/^{86}Sr$ levels in sea water, we observe that the acceleration of major icehouse periods, coincides with a reduction in plate tectonic activity in the late Cenozoic (~35 Ma) and Carboniferous (~325 Ma) (Fig. 10). We speculate that the icehouses may therefore have been regulated by changes in volcanic degassing and resulting cooling of the climate. Positive feedback mechanisms between continental ice formation and eustatic sea level may also have played an important role. A reduction of plate tectonic activity means less mid-ocean-ridge spreading, an increasing average depth of oceans, and therefore the lowering of eustatic sea level. The drying up of continental shelves leads to an increase in the albedo effect, potentially cooling Earth's climate further, consistent with fully coupled ocean-atmosphere model simulations (Farnsworth et al., 2019). As the Earth cools the area of continental ice increases, reducing eustatic sea level further and increasing the albedo – a 'snowball earth' like situation that would ultimately be limited by a drop in chemical weathering of silicate rocks (Le Hir et al., 2008; Pierrehumbert et al., 2011) and, in the Phanerozoic, by higher insolation at lower latitudes. In addition, a reduction in plate tectonic activity would result in less volcanic $CO_2$ degassing from spreading and subduction zones, which would ultimately reduce the levels of $CO_2$ in the atmosphere and cool the climate.

As was pointed out in the paleo-temperature reconstruction of Scotese et al. (2021), there appears to be a remarkably good correlation between the global temperature (Scotese et al. 2021) and non-radiogenic strontium flux (=plate tectonic activity) (van der Meer et al. 2017), which were derived independently. For 65 % of the Phanerozoic, when the ratio of $^{87}Sr/^{86}Sr$ in the oceans rose or fell (red line), global temperatures also rose or fell (Scotese et al. 2021). It is therefore not surprising that major ice sheet formation as derived here, is associated with a decrease in plate tectonic activity (Fig. 10).

At other times (i.e., late Permian), a significant reduction of plate tectonic activity did not result in creation of major ice sheets. Other factors may have played a major role in regulating Permian climate, such as net removal of $CO_2$ through the burial of organic carbon, and the enhancement of silicate weathering through the action of the terrestrial biosphere or the changes in the geographic location of weatherable silicate rocks e.g.(Berner, 2004; Goddéris et al., 2014; Kent and Muttoni, 2013). In addition, land may not have been positioned at the higher latitudes and therefore not favourable for the formation of large ice sheets.

Our analyses suggest that during the melting of Late Paleozoic ice sheets and hence a major rise in eustatic sea level (300–270 Ma), a major sea level fall (−100 m) occurred during the late Permian-early Triassic (~260–245 Ma) from changes in oceanic crustal production. The Permo-Triassic has been described to be the greatest Phanerozoic regression, with its effects particularly marked in the northern hemisphere, where shelf areas were nearly completely exposed (Yin et al., 2007), The amplitude of the end-Permian sea level fall has been quantified by Yasheng and Jiasong (2003), who measured the minimum meteoric dissolution of reefs in South China at 89.3 m. This fits well with our estimate.

### 3.2. Residual sea level trends (few to 20 million years) comparison

In the following section we will describe our residual shorter-term results of the tectono-glacial eustatic curve with a 60 Myr running average subtracted. This interval is like the time interval used for the long-term paleo-temperature reconstruction of Scotese et al. (2021). We note that our analyses would yield similar

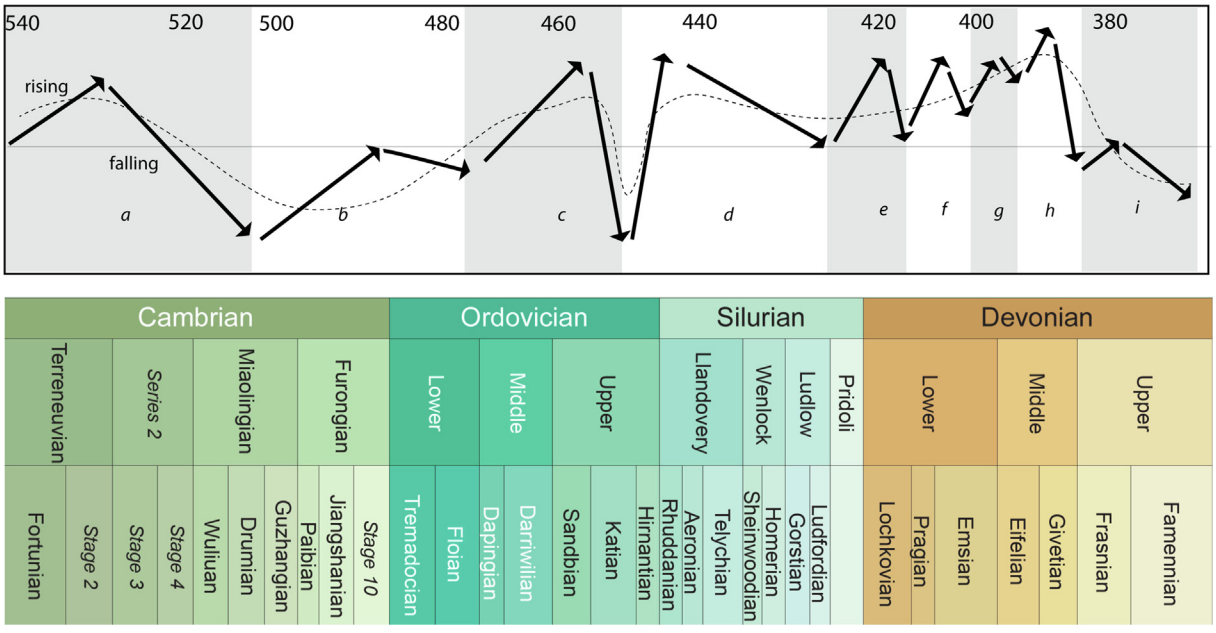


**Fig. 12. Cambrian-Devonian tectono-glacio-eustasy.** Dotted lines are the long-term (>50 Myr) eustatic trends. Up-arrows indicate medium-term rising sea level. Down-arrows indicate medium-term falling sea level. The numbers, letters and shading highlight the major, unconformity-bound stratigraphic sequences (see Supplementary Table 2 for details).

results for any subtraction between 45 and 70 Myr running averages. In Figs. 12-14, our eustatic sea level curve has been simplified to show only the major transgressive / regressive couplets. The associated amplitude changes are only schematically represented; for estimates of absolute values of sea level change, see Figs. 10 and 11. The letters, numbers, and shading highlight major, unconformity-bound stratigraphic sequences (see Supplementary Table 2 for details). 27 Transgressive-regressive couplets characterize our tectono-glacial eustatic (TGE) curve. We have used the ICS 2020 timescale to make geological stage assignments.

### 3.2.1. Cambrian and Ordovician

Though we do not discuss it explicitly here, eustatic sea level during late Neoproterozoic cold periods must have been very low (lower than −200 m) due to several episodes of intense "Snowball Earth" icehouse hypothesis (e.g. Hoffman et al., 1998; Pierrehumbert et al., 2011). According to this hypothesis, ice covered much of the continents and the sedimentary hiatus known as the "Great Unconformity" is found beneath Cambrian strata, worldwide (Keller et al., 2019; Peters and Gaines, 2012). Our eustatic curve (Fig. 12) shows that during the early and middle Cambrian rising sea levels flooded the continents. The tectono-glacial eustatic (TGE) curve indicates that eustatic sea level fell dramatically during the late Cambrian and then rose steadily through the Ordovician (see Supplementary Table 2). Our curve captures the dramatic fall in sea level during the Hirnantian Ice Age caused by the build-up of vast central Gondwanan ice sheets that extended into the subtropics.

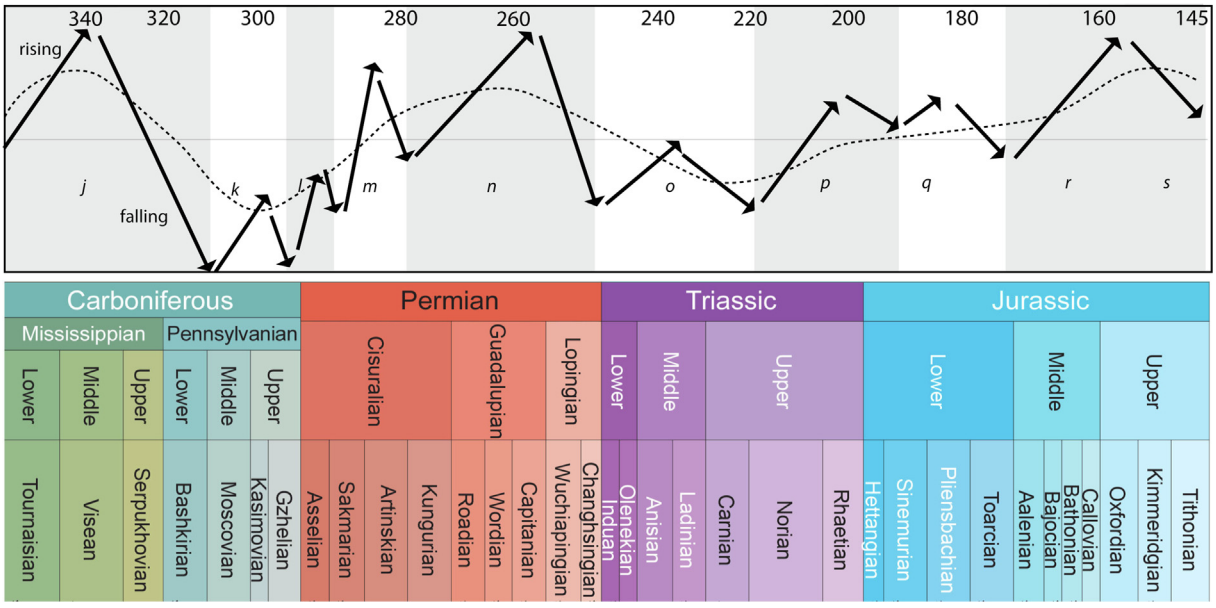


**Fig. 13. Carboniferous-Jurassic tectono-glacio-eustasy.** Up-arrows indicate rising sea level. Down-arrows indicate falling sea level. The numbers, letters and shading highlight the major, unconformity-bound stratigraphic sequences (see Supplementary Table 2). The dotted lines are the long-term (>50 Myr) eustatic trends.

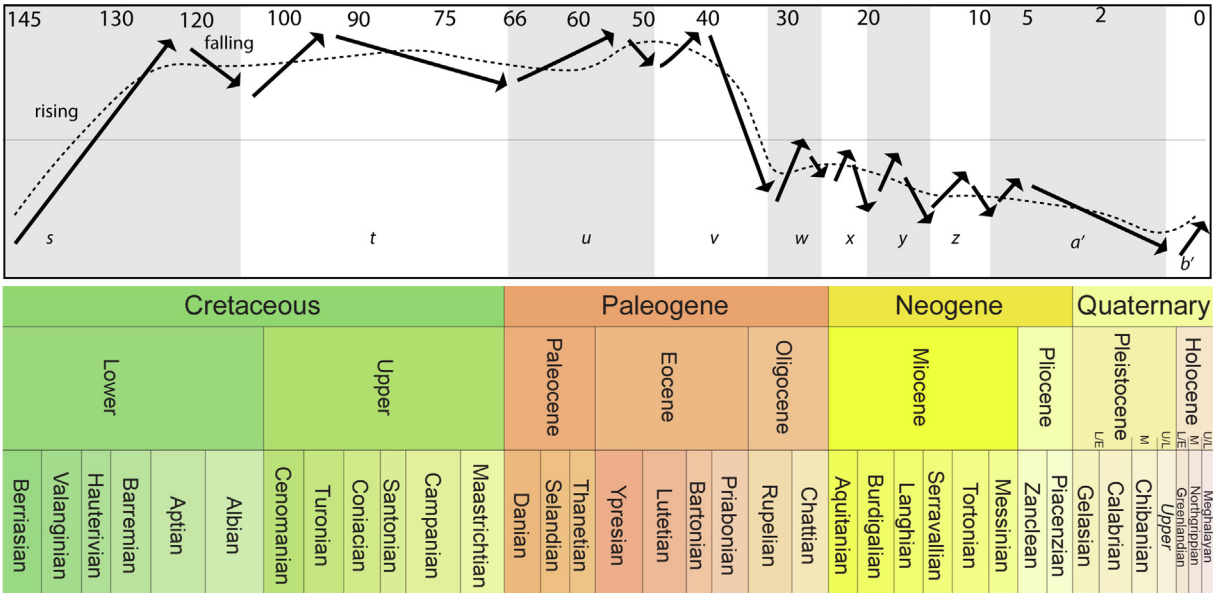


**Fig. 14. Cretaceous-Quaternary tectono-glacio-eustasy.** Up-arrows indicate rising eustatic sea level. Down-arrows indicate eustatic falling sea level. The numbers, letters and shading highlight the major, unconformity-bound stratigraphic sequences (see Supplementary Table 2 for details). The dotted lines are the long-term (>50 Myr) eustatic trends.

*3.2.2. Silurian and Devonian*

The Hirnantian eustatic event was short-lived. The Hirnantian Ice Age (Finnegan et al., 2011) lasted only a few million years; rising sea level reflooded the continents during the earliest Silurian (Llandovery, 440 Ma). Our TGE curve (Fig. 12) shows generally increasing sea levels during the Silurian and Devonian and indicate that maximum Paleozoic sea levels occurred during the middle Devonian (Givetian- early Frasnian; 385 Ma). It is likely that some of the eustatic sea level variations during the Silurian and Devonian were driven by the waxing and waning of relatively small south polar ice caps (e.g., the mid-Ludfordian glaciation (Frýda et al., 2021)). The best evidence of for these glacial episodes can be found in the latest Famennian tillites of the Amazon and Paranaiba basins (Caputo et al., 2008). Our TGE curve shows a fall in sea level during the late Silurian and the late Famennian (360 Ma).

*3.2.3. Carboniferous and Permian*

On the TGE curve there is a single eustatic peak at 340 Ma (Fig. 13). A dramatic fall in eustatic sea level took place near the end of the Mississippian (latest Serpukhovian, 325 Ma). Eustatic sea level remained low throughout the late Carboniferous and into the early Permian (~295 Ma), followed by a sharp drop in eustatic sea level at the beginning and the end of the Asselian (earliest Permian; 300–295 Ma) related to the Permo-Carboniferous glacial maximum. The TGE curve shows the sea level rising during the early Permian.

*3.2.4. Triassic and Jurassic*

Eustatic sea level fell precipitously during the late Permian and earliest Triassic (265–245 Ma, Fig. 13) then began to rise again at the start of the Middle Triassic (Anisian and early Ladinian. ~245 Ma). The TGE curve peaks during the Ladinian and falls during the early Late Triassic. It reverses direction at ~222 Ma and continues to rise into the Rhaetian.

The TGE curve indicates that sea level fell across the Triassic-Jurassic boundary. Continental deposits are dominant in the late Triassic of Europe. Marine deposits return in the Pliensbachian i. e. Scotese (2021). Eustatic sea level was low during the Early Jurassic and gradually rose during the remainder of the period. The Early Jurassic was one of the coolest time intervals during the Mesozoic. Glendonites and dropstones have been interpreted as evidence of cool climates at high southerly latitudes (Australia) (Boucot et al., 2013). Following the eustatic sea level low during most of the Early Jurassic (Hettangian-Sinemurian), eustatic sea level is estimated to rise during the latest Early Jurassic, peaking during the late Pliensbachian - early Toarcian (~183 Ma). After a brief retreat in the late Toarcian (~175 Ma), eustatic sea level increases dramatically during the middle Jurassic, reaching a maximum for the period during the Oxfordian-Kimmeridgian (~165 Ma). This was followed by eustatic sea level falling across the Jurassic-Cretaceous boundary.

*3.2.5. Cretaceous*

It has been inferred that glacio-eustasy was the likely driver of significant short-term eustatic sea level changes during the Cretaceous (Ray et al., 2019). The Cretaceous portions of both eustatic curves begin with a lowstand in sea level during Berriasian (145–140 Ma). Changes in eustatic sea level during the Early Cretaceous may have been driven by small, ephemeral glacio-eustatic events. Areas prone to ice sheet formation, were up to 8.3 million km$^2$ in extent (Fig. 7). In comparison, ice sheets of this size would cover ~58 % the area of Antarctica (14.2 million km$^2$) at maximum. Limited geological evidence of continental ice (tillites) exist in these times; in Australia during the Valanginian-Aptian (Alley et al., 2020) and in Siberia, Svalbard, and the Arctic Islands during the Berriasian – Barremian (Boucot et al., 2013; Cao et al., 2019; Price, 1999).

Eustatic sea level rose through the latter part of the early Cretaceous (Valanginian – Hauterivian, 140–125 Ma, Fig. 14) reaching a substantial peak in the Barremian-Aptian (125–120 Ma). A fall in eustatic sea level at the end of the Aptian (~115 Ma) may be related to the growth of a small polar ice cap during the Aptian-Albian "cold-snap" (O'Brien et al., 2017; Podlaha et al., 1998).

Eustatic sea level remains high throughout the remainder of the Cretaceous with a prominent eustatic sea level high near the Cenomanian/Turonian boundary (94 Ma). Eustatic sea level subsequently falls following the C-T highstand, before rebounding in the early Cenozoic.

*3.2.6. Cenozoic*

Our tectono-glacial curve (Fig. 14) may show four medium-term eustatic events during the Cenozoic. These four events are: a continuation of the highstands of eustatic sea level that characterized the Late Cretaceous into the Eocene, a peak in eustatic sea level during the early Eocene (50 Ma) followed by a steady fall in eustatic sea level during the middle and late Eocene, a precipitous drop in eustatic sea level at the Eocene/Oligocene boundary associated with the rapid growth of the Antarctic ice cap, and a continued fall in eustatic sea level during the Neogene and Quaternary due to the accumulation of continental ice at both poles.

*3.3. Future improvements*

1) Factors not explicitly included here may also be important, which require further analyses. Listing potential improvements from long-term tectonic to shorter-term sedimentary scale, we identify-five areas of improvement for obtaining a more accurate Phanerozoic eustatic sea level curve.
2) We assume that the volume of water available to fill the ocean basins has remained constant during Phanerozoic. Earth's lower mantle may store about five times more $H_2O$ than the oceans (Murakami et al., 2002). The flux rate between lower mantle and oceans may be significant as some of the present-day ocean water volume may have been temporarily stored in the mantle. In the recent Young et al. (2022) model, ocean water has been assumed to be stored in the mantle in a near-linear way, leading to an overall eustatic sea level fall of over 400 m + meter during the Phanerozoic.
3) In our model, the area of continental and oceanic crust is constant through time. It is a widely held belief that since the Archean, the volume and area of continental crust has continued to increase – possibly as much as ~15 % since the start the Phanerozoic (Scotese & Wright, 2018). If this is the case, then oceanic areas may have been larger in the Paleozoic and therefore, the ocean basins would have been able to store more water. This would suggest that we may have overestimated Paleozoic eustatic sea level in our curves and could therefore have been lower.
4) Assess any potential modifications to the strontium isotope derived plate tectonic estimate of van der Meer et al. (2017), i.e., incorporating the non-radiogenic strontium input from Large Igneous Provinces (LIPs). Therefore, at LIP eruption times and subsequent erosion, rate of sea floor spreading at mid ocean ridges may have been overestimated. This would lead to shallower ocean depth, and hence higher estimated values of our sea level. It may be due to specific circumstances of the eruption or erosion of the Siberian LIP that additional input of non-radiogenic strontium is not leading to a calculated sea level rise, or it is overwhelmed by another, yet unidentified process, or erosion of LIPs are only a small factor into the overall global balance of $^{87}Sr/^{86}Sr$ of the world's oceans. A more detailed modelling

study is required to determine why this LIP (and other, smaller LIPs), do not seem to be causing a notable offset in $^{87}Sr/^{86}Sr$, despite a relatively short Sr residence time in the oceans during this time (Vollstaedt et al., 2014).

5) Another factor which requires further study is the amount of continental ice. Stap et al. 2017, did not distinguish between land ice or grounded ice on the continental shelf, and derives net ice effects directly from sea level changes during the Last Glacial Maximum. Although our calculations are therefore reasonably calibrated in the late Cenozoic, unfortunately no similar climate-ice sheet model is available for (minor) Mesozoic and (major) Paleozoic glaciations. For example, ice sheets may have been thinner or thicker than our assumed averages, as derived from the late Cenozoic. We envision that future work will be able to further our approach using better temperature and ice volume reconstruction.
6) Hypsometry likely has changed in the past, but thus far we have linearly approximated the shelf margin's hypsometry, both for grounded ice estimates and to attribute eustatic sea level higher than Present-day. As noted in the paragraph on the tectonic component of eustasy, there may have been times when continents or shelf margins may have been steeper or shallower. Shelf hypsometry changes as a result of (glacio-)eustasy, i.e.,Sømme et al. (2009) or under the influence of large scale dynamic topography (Marcilly et al., 2022). Conceptual models based on modern relatively wide shelves may be poor predictors of (greenhouse) paleogeography (Burgess et al., 2022). More detailed analyses are required to assess these variations to our linearly approximated, fixed in time, hypsometry.

## 4. Conclusions

Phanerozoic eustatic sea level is a very important metric but global mean sea level is poorly constrained, resulting in large differences between estimates based on stratigraphically derived and plate tectonic studies (i.e. Simmons et al., 2020; van der Meer et al., 2017; Young et al., 2022). Here, we combine an updated estimate of plate tectonic activity (i.e., sea floor spreading and subduction) derived from the $^{87}Sr/^{86}Sr$ record of seawater (van der Meer et al., 2017) with a new measure of glacio-eustasy based on a recent model of Phanerozoic paleotemperatures (Scotese et al., 2021). Polar temperatures are used to predict the changing area of continental ice formation, which is then calibrated with a paleo-climate model for the late Cenozoic ice-house (Stap et al., 2017) to obtain ice thickness. We arrive at an average ~1.4 km thickness for ice sheets over 1Myr intervals. These glacio-eustatic effects, at medium-long term timescales (few – 50 + Myr) lead to eustatic changes of up to ~90 m. We have combined the glacio-eustatic effects with changes in the ocean volume derived from our tectonic estimate to obtain a Tectono-Glacio-Eustatic curve for the entire Phanerozoic.

## Declaration of Competing Interest

The authors declare that they have no known competing financial interests or personal relationships that could have appeared to influence the work reported in this paper.

## Acknowledgements

DGvdM acknowledges his colleagues at CNOOC for the fruitful discussions over the past decade on sea level. AS thanks the European Research Council for Consolidator Grant 771497. BJWM is funded by the UK Natural Environment Research Council (NE/S009663/1).

## Appendix A. Supplementary material

Supplementary data to this article can be found online at https://doi.org/10.1016/j.gr.2022.07.014.

## References

Abreu, V.S., Hardenbol, J., Haddad, G.A., Baum, G.R., Droxler, A.W., Vail, P.R., 1998. Oxygen isotope synthesis: a Cretaceous ice-house?. SEPM (Soc. Sediment. Geol.), 75–80. https://doi.org/10.2110/pec.98.02.0075.
Allègre, C.J., Louvat, P., Gaillardet, J., Meynadier, L., Rad, S., Capmas, F., 2010. The fundamental role of island arc weathering in the oceanic Sr isotope budget. Earth Planet. Sci. Lett. 292, 51–56. https://doi.org/10.1016/j.epsl.2010.01.019.
Alley, N.F., Frakes, L.A., 2003. First known Cretaceous glaciation: Livingston Tillite Member of the Cadna-owie Formation, South Australia.. Aust. J. Earth Sci. 50, 139–144. https://doi.org/10.1046/j.1440-0952.2003.00984.x.
Alley, N.F., Hore, S.B., Frakes, L.A., 2020. Glaciations at high-latitude Southern Australia during the Early Cretaceous. Aust. J. Earth Sci. 67, 1045–1095. https://doi.org/10.1080/08120099.2019.1590457.
Amante, C., Eakins, B.W., 2009. ETOPO1 1 Arc-Minute Global Relief Model: Procedures, Data Sources and Analysis. NOAA Tech. Memo. NESDIS NGDC-24. https://doi.org/10.7289/V5C8276M.
Berner, R.A., 1991. A model for atmospheric CO sub 2 over phanerozoic time. Am. J. Sci. U. S. 291, 4. https://doi.org/10.2475/ajs.291.4.339.
Berner, R.A., 2004. The Phanerozoic Carbon Cycle: CO2 and O2. Oxford University Press, Oxford, New York.
Bintanja, R., van de Wal, R.S.W., 2008. North American ice-sheet dynamics and the onset of 100,000-year glacial cycles. Nature 454, 869–872. https://doi.org/10.1038/nature07158.
Boschman, L.M., van Hinsbergen, D.J.J., 2016. On the enigmatic birth of the Pacific Plate within the Panthalassa Ocean. Sci. Adv. 2, e1600022. https://doi.org/10.1126/sciadv.1600022.
Boschman, L.M., van Hinsbergen, D.J.J., Kimbrough, D.L., Langereis, C.G., Spakman, W., 2018. The Dynamic History of 220 Million Years of Subduction Below Mexico: A Correlation Between Slab Geometry and Overriding Plate Deformation Based on Geology, Paleomagnetism, and Seismic Tomography. Geochem. Geophys. Geosyst. 19, 4649–4672. https://doi.org/10.1029/2018GC007739.
Boucot, A.J., Xu, C., Scotese, C.R., Morley, R.J., 2013. Phanerozoic Paleoclimate: An Atlas of Lithologic Indicators of Climate. https://doi.org/10.2110/sepmcsp.11.
Browning, J.V., Miller, K.G., Pak, D.K., 1996. Global implications of lower to middle Eocene sequence boundaries on the New Jersey coastal plain: The icehouse cometh. Geology 24, 639–642. https://doi.org/10.1130/0091-7613(1996)024<0639:GIOLTM>2.3.CO;2.
Brune, S., Williams, S.E., Müller, R.D., 2017. Potential links between continental rifting, CO2 degassing and climate change through time. Nat. Geosci. 10, 941–946. https://doi.org/10.1038/s41561-017-0003-6.
Budyko, M.I., 1969. The effect of solar radiation variations on the climate of the Earth. Tellus 21, 611–619. https://doi.org/10.3402/tellusa.v21i5.10109.
Burgess, P.M., Moresi, L.N., 1999. Modelling rates and distribution of subsidence due to dynamic topography over subducting slabs: is it possible to identify dynamic topography from ancient strata?. Basin Res. 11, 305–314.
Burgess, P.M., Prince, G.D., 2015. Non-unique stratal geometries: implications for sequence stratigraphic interpretations. Basin Res. 27, 351–365. https://doi.org/10.1111/bre.12082.
Burgess, P.M., Zhang, J., Steel, R., 2022. Narrow is normal: Exploring the extent and significance of flooded marine shelves in icehouse, transitional, and greenhouse climate settings. Geology 50 (4), 496–499.
Burton, R., Kendall, C.G., St, C., Lerche, I., 1987. Out of our depth: on the impossibility of fathoming eustasy from the stratigraphic record. Earth-Sci. Rev. 24, 237–277. https://doi.org/10.1016/0012-8252(87)90062-6.
Butterworth, N.P., Talsma, A.S., Müller, R.D., Seton, M., Bunge, H.-P., Schuberth, B.S.A., Shephard, G.E., Heine, C., 2014. Geological, tomographic, kinematic and geodynamic constraints on the dynamics of sinking slabs. J. Geodyn. 73, 1–13. https://doi.org/10.1016/j.jog.2013.10.006.
Caldeira, K., Kasting, J.F., 1992. The life span of the biosphere revisited. Nature 360, 721–723. https://doi.org/10.1038/360721a0.
Cao, W., Williams, S., Flament, N., Zahirovic, S., Scotese, C., Müller, R.D., 2019. Palaeolatitudinal distribution of lithologic indicators of climate in a palaeogeographic framework. Geol. Mag. 156, 331–354. https://doi.org/10.1017/S0016756818000110.
Caputo, M.V., Melo, J.H., Streel, M., Isbell, J.L., 2008. Late Devonian and Early Carboniferous glacial records of South America. Spec. Pap. Geol. Soc. Am. 441. https://doi.org/10.1130/2008.2441(11).
Cloetingh, S., Haq, B.U., 2015. Inherited landscapes and sea level change. Science 347, 1258375. https://doi.org/10.1126/science.1258375.
Coltice, N., Seton, M., Rolf, T., Müller, R.D., Tackley, P.J., 2013. Convergence of tectonic reconstructions and mantle convection models for significant fluctuations in seafloor spreading. Earth Planet. Sci. Lett. 383, 92–100. https://doi.org/10.1016/j.epsl.2013.09.032.

Conrad, C.P., 2013. The solid Earth's influence on sea level. Geol. Soc. Am. Bull. 125, 1027–1052. https://doi.org/10.1130/B30764.1.
Cramwinckel, M.J., Huber, M., Kocken, I.J., Agnini, C., Bijl, P.K., Bohaty, S.M., Frieling, J., Goldner, A., Hilgen, F.J., Kip, E.L., Peterse, F., van der Ploeg, R., Röhl, U., Schouten, S., Sluijs, A., 2018. Synchronous tropical and polar temperature evolution in the Eocene. Nature 559, 382–386. https://doi.org/10.1038/s41586-018-0272-2.
Crowley, T.J., Burke, K., 1998. Tectonic Boundary Conditions for Climate Reconstructions. Oxford University Press.
Davies, A., Gréselle, B., Hunter, S.J., Baines, G., Robson, C., Haywood, A.M., Ray, D.C., Simmons, M.D., van Buchem, F.S.P., 2020. Assessing the impact of aquifer-eustasy on short-term Cretaceous sea-level. Cretac. Res. 112,. https://doi.org/10.1016/j.cretres.2020.104445 104445.
de Bar, M.W., de Nooijer, L.J., Schouten, S., Ziegler, M., Sluijs, A., Reichart, G.-J., 2019. Comparing Seawater Temperature Proxy Records for the Past 90 Myrs From the Shallow Shelf Record Bass River, New Jersey. Paleoceanogr. Paleoclimatol. 34, 455–475. https://doi.org/10.1029/2018PA003453.
de Boer, B., van de Wal, R.S.W., Bintanja, R., Lourens, L.J., Tuenter, E., 2010. Cenozoic global ice-volume and temperature simulations with 1-D ice-sheet models forced by benthic δ18O records. Ann. Glaciol. 51, 23–33. https://doi.org/10.3189/172756410791392736.
DeConto, R.M., Pollard, D., 2003. Rapid Cenozoic glaciation of Antarctica induced by declining atmospheric CO2. Nature 421, 245–249. https://doi.org/10.1038/nature01290.
DeConto, R.M., Pollard, D., Wilson, P.A., Pälike, H., Lear, C.H., Pagani, M., 2008. Thresholds for Cenozoic bipolar glaciation. Nature 455, 652–656. https://doi.org/10.1038/nature07337.
Domeier, M., Shephard, G.E., Jakob, J., Gaina, C., Doubrovine, P.V., Torsvik, T.H., 2017. Intraoceanic subduction spanned the Pacific in the Late Cretaceous-Paleocene. Sci. Adv. 3, eaao2303. https://doi.org/10.1126/sciadv.aao2303.
Domeier, M., Torsvik, T.H., 2017. Full-plate modelling in pre-Jurassic time. Geol. Mag. 156, 261–280. https://doi.org/10.1017/S0016756817001005.
Douglas, P.M.J., Affek, H.P., Ivany, L.C., Houben, A.J.P., Sijp, W.P., Sluijs, A., Schouten, S., Pagani, M., 2014. Pronounced zonal heterogeneity in Eocene southern high-latitude sea surface temperatures. Proc. Natl. Acad. Sci. 111, 6582–6587. https://doi.org/10.1073/pnas.1321441111.
Farnsworth, A., Lunt, D.J., O'Brien, C.L., Foster, G.L., Inglis, G.N., Markwick, P., Pancost, R.D., Robinson, S.A., 2019. Climate Sensitivity on Geological Timescales Controlled by Nonlinear Feedbacks and Ocean Circulation. Geophys. Res. Lett. 46, 9880–9889. https://doi.org/10.1029/2019GL083574.
Farrell, W.E., Clark, J.A., 1976. On Postglacial Sea Level. Geophys. J. Int. 46, 647–667. https://doi.org/10.1111/j.1365-246X.1976.tb01252.x.
Finnegan, S., Bergmann, K., Eiler, J.M., Jones, D.S., Fike, D.A., Eisenman, I., Hughes, N. C., Tripati, A.K., Fischer, W.W., 2011. The Magnitude and Duration of Late Ordovician-Early Silurian Glaciation. Science 331, 903–906. https://doi.org/10.1126/science.1200803.
Foster, G.L., Royer, D.L., Lunt, D.J., 2017. Future climate forcing potentially without precedent in the last 420 million years. Nat. Commun. 8, 14845. https://doi.org/10.1038/ncomms14845.
Frieling, J., Gebhardt, H., Huber, M., Adekeye, O.A., Akande, S.O., Reichart, G.-J., Middelburg, J.J., Schouten, S., Sluijs, A., 2017. Extreme warmth and heat-stressed plankton in the tropics during the Paleocene-Eocene Thermal Maximum. Sci. Adv. 3, e1600891.
Frýda, J., Lehnert, O., Joachimski, M.M., Männik, P., Kubajko, M., Mergl, M., Farkaš, J., Frýdová, B., 2021. The Mid-Ludfordian (late Silurian) Glaciation: A link with global changes in ocean chemistry and ecosystem overturns. Earth-Sci. Rev. 220,. https://doi.org/10.1016/j.earscirev.2021.103652 103652.
Goddéris, Y., Donnadieu, Y., Le Hir, G., Lefebvre, V., Nardin, E., 2014. The role of palaeogeography in the Phanerozoic history of atmospheric CO2 and climate. Earth-Sci. Rev. 128, 122–138. https://doi.org/10.1016/j.earscirev.2013.11.004.
Grand, S., van der Hilst, R.D., Widiyantoro, S., 1997. Global seismic tomography: a snapshot of convection in the earth. GSA Today 7, 1–7.
Hallam, A., 1984. Pre-Quaternary Sea-Level Changes. Annu. Rev. Earth Planet. Sci. 12, 205–243. https://doi.org/10.1146/annurev.ea.12.050184.001225.
Hansen, J., Sato, M., Russell, G., Kharecha, P., 2013. Climate sensitivity, sea level and atmospheric carbon dioxide. Philos. Trans. R. Soc. Math. Phys. Eng. Sci. 371, 20120294. https://doi.org/10.1098/rsta.2012.0294.
Haq, B.U., 2014. Cretaceous eustasy revisited. Glob. Planet. Change 113, 44–58. https://doi.org/10.1016/j.gloplacha.2013.12.007.
Haq, B.U., 2018a. Jurassic Sea-Level Variations: A Reappraisal. GSA Today 28, 4–10. https://doi.org/10.1130/GSATG359A.1.
Haq, B.U., 2018b. Triassic Eustatic Variations Reexamined. GSA Today 28, 4–9. https://doi.org/10.1130/GSATG381A.1.
Haq, B.U., Al-Qahtani, A.M., 2005. Phanerozoic cycles of sea-level change on the Arabian Platform. GeoArabia 10, 127–160. https://doi.org/10.2113/geoarabia1002127.
Haq, B.U., Hardenbol, J., Vail, P.R., 1987. Chronology of Fluctuating Sea Levels Since the Triassic. Science 235, 1156–1167. https://doi.org/10.1126/science.235.4793.1156.
Haq, B.U., Schutter, S.R., 2008. A Chronology of Paleozoic Sea-Level Changes. Science 322, 64–68. https://doi.org/10.1126/science.1161648.
Hays, J.D., Imbrie, J., Shackleton, N.J., 1976. Variations in the Earth's Orbit: Pacemaker of the Ice Ages. Science 194, 1121–1132. https://doi.org/10.1126/science.194.4270.1121.
Hirt, C., Rexer, M., 2015. Earth 2014: 1 arc-min shape, topography, bedrock and ice-sheet models – Available as gridded data and degree-10,800 spherical harmonics. Int. J. Appl. Earth Obs. Geoinform. 39, 103–112. https://doi.org/10.1016/j.jag.2015.03.001.
Hoffman, P.F., Kaufman, A.J., Halverson, G.P., Schrag, D.P., 1998. A Neoproterozoic Snowball Earth. Science 281 (5381), 1342–1346.
Karlsen, K.S., Domeier, M., Gaina, C., Conrad, C.P., 2020. A tracer-based algorithm for automatic generation of seafloor age grids from plate tectonic reconstructions. Comput. Geosci. 140,. https://doi.org/10.1016/j.cageo.2020.104508 104508.
Keller, C.B., Husson, J.M., Mitchell, R.N., Bottke, W.F., Gernon, T.M., Boehnke, P., Bell, E.A., Swanson-Hysell, N.L., Peters, S.E., 2019. Neoproterozoic glacial origin of the Great Unconformity. Proc. Natl. Acad. Sci. 116, 1136–1145. https://doi.org/10.1073/pnas.1804350116.
Kent, D.V., Muttoni, G., 2013. Modulation of Late Cretaceous and Cenozoic climate by variable drawdown of atmospheric pCO2 from weathering of basaltic provinces on continents drifting through the equatorial humid belt. Clim. Past 9, 525–546. https://doi.org/10.5194/cp-9-525-2013.
Kominz, M.A., Browning, J.V., Miller, K.G., Sugarman, P.J., Mizintseva, S., Scotese, C.R., 2008. Late Cretaceous to Miocene sea-level estimates from the New Jersey and Delaware coastal plain coreholes: an error analysis. Basin Res. 20, 211–226. https://doi.org/10.1111/j.1365-2117.2008.00354.x.
Kominz, M.A., Miller, K.G., Browning, J.V., Katz, M.E., Mountain, G.S., 2016. Miocene relative sea level on the New Jersey shallow continental shelf and coastal plain derived from one-dimensional backstripping: A case for both eustasy and epeirogeny. Geosphere 12, 1437–1456. https://doi.org/10.1130/GES01241.1.
Lambeck, K., Chappell, J., 2001. Sea Level Change Through the Last Glacial Cycle. Science 292, 679–686. https://doi.org/10.1126/science.1059549.
Le Hir, G., Ramstein, G., Donnadieu, Y., Goddéris, Y., 2008. Scenario for the evolution of atmospheric pCO2 during a snowball Earth. Geology 36, 47–50. https://doi.org/10.1130/G24124A.1.
Lear, C.H., Elderfield, H., Wilson, P.A., 2000. Cenozoic Deep-Sea Temperatures and Global Ice Volumes from Mg/Ca in Benthic Foraminiferal Calcite. Science 287, 269–272. https://doi.org/10.1126/science.287.5451.269.
Lenton, T.M., 2001. The role of land plants, phosphorus weathering and fire in the rise and regulation of atmospheric oxygen. Glob. Change Biol. 7, 613–629. https://doi.org/10.1046/j.1354-1013.2001.00429.x.
Liu, L., 2015. The ups and downs of North America: Evaluating the role of mantle dynamic topography since the Mesozoic. Rev. Geophys. 53, 1022–1049. https://doi.org/10.1002/2015RG000489.
Liu, L., Spasojević, S., Gurnis, M., 2008. Reconstructing Farallon Plate subduction beneath North America back to the Late Cretaceous. Science 322 (5903), 934–938.
Marcilly, C.M., Torsvik, T.H., Conrad, C.P., 2022. Global Phanerozoic sea levels from paleogeographic flooding maps. Gondwana Res. 110, 128–142.
Matthews, K.J., Maloney, K.T., Zahirovic, S., Williams, S.E., Seton, M., Müller, R.D., 2016. Global plate boundary evolution and kinematics since the late Paleozoic. Glob. Planet. Change 146, 226–250. https://doi.org/10.1016/j.gloplacha.2016.10.002.
McArthur, J.M., Howarth, R.J., Shields, G.A., 2012. Strontium Isotope Stratigraphy. In: Gradstein, F.M., Ogg, J.G., Schmotz, M.D., Ogg, G.M. (Eds.), The Geological Time Scale 2012. Elsevier, pp. 127–144.
McArthur, J.M., Howarth, R.J., Shields, G.A., Zhou, Y., 2020. Chapter 7 - Strontium Isotope Stratigraphy. In: Gradstein, F.M., Ogg, J.G., Schmitz, M.D., Ogg, G.M. (Eds.), Geologic Time Scale 2020. Elsevier, pp. 211–238. https://doi.org/10.1016/B978-0-12-824360-2.00007-3.
Miall, A.D. (Ed.), 2010. The Geology of Stratigraphic Sequences. Springer Berlin Heidelberg, Berlin, Heidelberg.
Milanković, M., 1941. Canon of insolation and the ice-age problem (Kanon der Erdbestrahlung und seine Anwendung auf das Eiszeitenproblem). K. Serb. Akad. Beogr. Spec. Publ, Belgrade.
Miller, K.G., Kominz, M.A., Browning, J.V., Wright, J.D., Mountain, G.S., Katz, M.E., Sugarman, P.J., Cramer, B.S., Christie-Blick, N., Pekar, S.F., 2005. The Phanerozoic Record of Global Sea-Level Change. Science 310, 1293–1298. https://doi.org/10.1126/science.1116412.
Miller, K.G., Browning, J.V., Schmelz, W.J., Kopp, R.E., Mountain, G.S., Wright, J.D., 2020. Cenozoic sea-level and cryospheric evolution from deep-sea geochemical and continental margin records. Sci. Adv. 6, eaaz1346. https://doi.org/10.1126/sciadv.aaz1346.
Mills, B.J.W., Daines, S.J., Lenton, T.M., 2014. Changing tectonic controls on the long-term carbon cycle from Mesozoic to present. Geochem. Geophys. Geosyst. 15, 4866–4884. https://doi.org/10.1002/2014GC005530.
Mills, B.J.W., Krause, A.J., Scotese, C.R., Hill, D.J., Shields, G.A., Lenton, T.M., 2019. Modelling the long-term carbon cycle, atmospheric CO2, and Earth surface temperature from late Neoproterozoic to present day. Gondwana Res. 67, 172–186. https://doi.org/10.1016/j.gr.2018.12.001.
Mills, B.J.W., Donnadieu, Y., Goddéris, Y., 2021. Spatial continuous integration of Phanerozoic global biogeochemistry and climate. Gondwana Res. 100, 73–86. https://doi.org/10.1016/j.gr.2021.02.011.
Moucha, R., Forte, A.M., Mitrovica, J.X., Rowley, D.B., Quéré, S., Simmons, N.A., Grand, S.P., 2008. Dynamic topography and long-term sea-level variations: There is no such thing as a stable continental platform. Earth Planet. Sci. Lett. 271, 101–108. https://doi.org/10.1016/j.epsl.2008.03.056.
Müller, R.D., Hassan, R., Gurnis, M., Flament, N., Williams, S.E., 2018. Dynamic topography of passive continental margins and their hinterlands since the Cretaceous.. Gondwana Res. 53, 225–251. https://doi.org/10.1016/j.gr.2017.04.028.

Müller, R.D., Sdrolias, M., Gaina, C., Steinberger, B., Heine, C., 2008. Long-Term Sea-Level Fluctuations Driven by Ocean Basin Dynamics. Science 319, 1357–1362. https://doi.org/10.1126/science.1151540.

Müller, R.D., Seton, M., Zahirovic, S., Williams, S.E., Matthews, K.J., Wright, N.M., Shephard, G.E., Maloney, K.T., Barnett-Moore, N., Hosseinpour, M., Bower, D.J., Cannon, J., 2016. Ocean Basin Evolution and Global-Scale Plate Reorganization Events Since Pangea Breakup. Annu. Rev. Earth Planet. Sci. 44, 107–138. https://doi.org/10.1146/annurev-earth-060115-012211.

Müller, R.D., Zahirovic, S., Williams, S.E., Cannon, J., Seton, M., Bower, D.J., Tetley, M. G., Heine, C., Breton, E.L., Liu, S., Russell, S.H.J., Yang, T., Leonard, J., Gurnis, M., 2019. A Global Plate Model Including Lithospheric Deformation Along Major Rifts and Orogens Since the Triassic. Tectonics 38, 1884–1907. https://doi.org/10.1029/2018TC005462.

Murakami, M., Hirose, K., Yurimoto, H., Nakashima, S., Takafuji, N., 2002. Water in Earth's Lower Mantle. Science 295, 1885–1887. https://doi.org/10.1126/science.1065998.

Nance, R.D., Murphy, J.B., 2019. Supercontinents and the case for Pannotia. Geol. Soc. Lond. Spec. Publ. 470, 65–86. https://doi.org/10.1144/SP470.5.

Norton, I.O., Lawver, L.A., 2014. Seawater chemistry driven by supercontinent assembly, breakup, and dispersal: COMMENT. Geology 42, e334–e. https://doi.org/10.1130/G35109C.1.

O'Brien, C.L., Robinson, S.A., Pancost, R.D., Sinninghe Damsté, J.S., Schouten, S., Lunt, D.J., Alsenz, H., Bornemann, A., Bottini, C., Brassell, S.C., Farnsworth, A., Forster, A., Huber, B.T., Inglis, G.N., Jenkyns, H.C., Linnert, C., Littler, K., Markwick, P., McAnena, A., Mutterlose, J., Naafs, B.D.A., Püttmann, W., Sluijs, A., van Helmond, N.A.G.M., Vellekoop, J., Wagner, T., Wrobel, N.E., 2017. Cretaceous sea-surface temperature evolution: Constraints from TEX86 and planktonic foraminiferal oxygen isotopes. Earth-Sci. Rev. 172, 224–247. https://doi.org/10.1016/j.earscirev.2017.07.012.

Parsons, B., 1982. Causes and consequences of the relation between area and age of the ocean floor. J. Geophys. Res. Solid Earth 87, 289–302. https://doi.org/10.1029/JB087iB01p00289.

Parsons, B., Sclater, J.G., 1977. An analysis of the variation of ocean floor bathymetry and heat flow with age. J. Geophys. Res. 82, 803–827. https://doi.org/10.1029/JB082i005p00803.

Peltier, W.R., Andrews, J.T., 1976. Glacial-Isostatic Adjustment—I. The Forward Problem. Geophys. J. Int. 46, 605–646. https://doi.org/10.1111/j.1365-246X.1976.tb01251.x.

Peters, S.E., Gaines, R.R., 2012. Formation of the 'Great Unconformity' as a trigger for the Cambrian explosion. Nature 484, 363–366. https://doi.org/10.1038/nature10969.

Pierrehumbert, R.T., Abbot, D.S., Voigt, A., Koll, D., 2011. Climate of the Neoproterozoic. Annu. Rev. Earth Planet. Sci. 39, 417–460. https://doi.org/10.1146/annurev-earth-040809-152447.

Podlaha, O., Mutterlose, J., Veizer, J., 1998. Preservation of δ18O and δ13C in Belemnite rostra from the Jurassic/Early Cretaceous successions. Am. J. Sci. 298, 324–347. https://doi.org/10.2475/ajs.298.4.324.

Price, G.D., 1999. The evidence and implications of polar ice during the Mesozoic. Earth-Sci. Rev. 48, 183–210. https://doi.org/10.1016/S0012-8252(99)00048-3.

Ray, D.C., van Buchem, F.S.P., Baines, G., Davies, A., Gréselle, B., Simmons, M.D., Robson, C., 2019. The magnitude and cause of short-term eustatic Cretaceous sea-level change: A synthesis. Earth-Sci. Rev. 197,. https://doi.org/10.1016/j.earscirev.2019.102901 102901.

Raymo, M.E., Mitrovica, J.X., O'Leary, M.J., DeConto, R.M., Hearty, P.J., 2011. Departures from eustasy in Pliocene sea-level records. Nat. Geosci. 4, 328–332. https://doi.org/10.1038/ngeo1118.

Rohling, E.J., Grant, K., Bolshaw, M., Roberts, A.P., Siddall, M., Hemleben, C., Kucera, M., 2009. Antarctic temperature and global sea level closely coupled over the past five glacial cycles. Nat. Geosci. 2, 500–504. https://doi.org/10.1038/ngeo557.

Rohling, E.J., Foster, G.L., Grant, K.M., Marino, G., Roberts, A.P., Tamisiea, M.E., Williams, F., 2014. Sea-level and deep-sea-temperature variability over the past 5.3 million years. Nature 508, 477–482. https://doi.org/10.1038/nature13230.

Rygel, M.C., Fielding, C.R., Frank, T.D., Birgenheier, L.P., 2008. The Magnitude of Late Paleozoic Glacioeustatic Fluctuations: A Synthesis. J. Sediment. Res. 78, 500–511. https://doi.org/10.2110/jsr.2008.058.

Saunders, W.B., Ramsbottom, W.H.C., 1986. The mid-Carboniferous eustatic event. Geology 14, 208–212. https://doi.org/10.1130/0091-7613(1986)14<208:TMEE>2.0.CO;2.

Sclater, J.G., Jaupart, C., Galson, D., 1980. The heat flow through oceanic and continental crust and the heat loss of the Earth. Rev. Geophys. 18, 269–311. https://doi.org/10.1029/RG018i001p00269.

Scotese, C.R., 2021. An Atlas of Phanerozoic Paleogeographic Maps: The Seas Come In and the Seas Go Out. Annu. Rev. Earth Planet. Sci. 49 (1), 679–728.

Scotese, C.R., Wright, N.M., 2018. PALEOMAP Paleodigital Elevation Models (PaleoDEMS) for the Phanerozoic PALEOMAP Project. Httpswwwearthbyteorgpaleodem-Resour.- -Wright-2018.

Scotese, C.R., Song, H., Mills, B.J.W., van der Meer, D.G., 2021. Phanerozoic paleotemperatures: The earth's changing climate during the last 540 million years. Earth-Sci. Rev. 215, 103503. https://doi.org/10.1016/j.earscirev.2021.103503.

Sellers, W.D., 1969. A Global Climatic Model Based on the Energy Balance of the Earth-Atmosphere System. J. Appl. Meteorol. Climatol. 8, 392–400. https://doi.org/10.1175/1520-0450(1969)008<0392:AGCMBO>2.0.CO;2.

Seton, M., Müller, R.D., Zahirovic, S., Gaina, C., Torsvik, T., Shephard, G., Talsma, A., Gurnis, M., Turner, M., Maus, S., Chandler, M., 2012. Global continental and ocean basin reconstructions since 200 Ma. Earth-Sci. Rev. 113, 212–270. https://doi.org/10.1016/j.earscirev.2012.03.002.

Shackleton, N., 1967. Oxygen Isotope Analyses and Pleistocene Temperatures Re-assessed. Nature 215, 15–17. https://doi.org/10.1038/215015a0.

Shackleton, N.J., Opdyke, N.D., 1973. Oxygen Isotope and Palaeomagnetic Stratigraphy of Equatorial Pacific Core V28–238: Oxygen Isotope Temperatures and Ice Volumes on a 105 Year and 106 Year Scale*. Quat. Res. 3, 39–55. https://doi.org/10.1016/0033-5894(73)90052-5.

Shackleton, N.J., Wiseman, J.D.H., Buckley, H.A., 1973. Non-equilibrium Isotopic Fractionation between Seawater and Planktonic Foraminiferal Tests. Nature 242, 177–179. https://doi.org/10.1038/242177a0.

Sherwood, S.C., Huber, M., 2010. An adaptability limit to climate change due to heat stress. Proc. Natl. Acad. Sci. 107, 9552–9555. https://doi.org/10.1073/pnas.0913352107.

Sigloch, K., Mihalynuk, M.G., 2013. Intra-oceanic subduction shaped the assembly of Cordilleran North America. Nature 496, 50–56. https://doi.org/10.1038/nature12019.

Simmons, M.D., Miller, K.G., Ray, D.C., Davies, A., van Buchem, F.S.P., Gréselle, B., 2020. Chapter 13 - Phanerozoic Eustasy. In: Gradstein, F.M., Ogg, J.G., Schmitz, M.D., Ogg, G.M. (Eds.), Geologic Time Scale 2020. Elsevier, pp. 357–400. https://doi.org/10.1016/B978-0-12-824360-2.00013-9.

Sluijs, A., Brinkhuis, H., Crouch, E.M., John, C.M., Handley, L., Munsterman, D., Bohaty, S.M., Zachos, J.C., Reichart, G.-J., Schouten, S., Pancost, R.D., Damsté, J.S.S., Welters, N.L.D., Lotter, A.F., Dickens, G.R., 2008. Eustatic variations during the Paleocene-Eocene greenhouse world. Paleoceanography 23 (4).

Sømme, T.O., Helland-Hansen, W., Granjeon, D., 2009. Impact of eustatic amplitude variations on shelf morphology, sediment dispersal, and sequence stratigraphic interpretation: Icehouse versus greenhouse systems. Geology 37, 587–590. https://doi.org/10.1130/G25511A.1.

Song, H., Wignall, P.B., Song, H., Dai, X., Chu, D., 2019. Seawater Temperature and Dissolved Oxygen over the Past 500 Million Years. J. Earth Sci. 30, 236–243. https://doi.org/10.1007/s12583-018-1002-2.

Spasojevic, S., Gurnis, M., 2012. Sea level and vertical motion of continents from dynamic earth models since the Late Cretaceous. AAPG Bull. 96, 2037–2064. https://doi.org/10.1306/03261211121.

Stap, L.B., van de Wal, R.S.W., de Boer, B., Bintanja, R., Lourens, L.J., 2014. Interaction of ice sheets and climate during the past 800 000 years. Clim. Past 10, 2135–2152. https://doi.org/10.5194/cp-10-2135-2014.

Stap, L.B., Wal, R.S.W., De Boer, B., Bintanja, R., Lourens, L., 2016a. The influence of ice sheets on the climate during the past 38 million years. Clim. Past Discuss. 1–18. https://doi.org/10.5194/cp-2016-109.

Stap, L.B., van de Wal, R.S.W., Boer, B.D., Bintanja, R., Lourens, L.J., 2016b. The MMCO-EOT conundrum: Same benthic δ18O, different CO2. Paleoceanography 31, 1270–1282. https://doi.org/10.1002/2016PA002958.

Stap, L.B., van de Wal, R.S.W., de Boer, B., Bintanja, R., Lourens, L.J., 2017. The influence of ice sheets on temperature during the past 38 million years inferred from a one-dimensional ice sheet–climate model. Clim. Past 13, 1243–1257. https://doi.org/10.5194/cp-13-1243-2017.

Stein, C.A., Stein, S., 1992. A model for the global variation in oceanic depth and heat flow with lithospheric age. Nature 359, 123–129. https://doi.org/10.1038/359123a0.

Stocchi, P., Escutia, C., Houben, A.J.P., Vermeersen, B.L.A., Bijl, P.K., Brinkhuis, H., DeConto, R.M., Galeotti, S., Passchier, S., Pollard, D., Brinkhuis, H., Escutia, C., Klaus, A., Fehr, A., Williams, T., Bendle, J.A.P., Bijl, P.K., Bohaty, S.M., Carr, S.A., Dunbar, R.B., Flores, J.A., Gonzàlez, J.J., Hayden, T.G., Iwai, M., Jimenez-Espejo, F. J., Katsuki, K., Kong, G.S., McKay, R.M., Nakai, M., Olney, M.P., Passchier, S., Pekar, S.F., Pross, J., Riesselman, C., Röhl, U., Sakai, T., Shrivastava, P.K., Stickley, C.E., Sugisaki, S., Tauxe, L., Tuo, S., van de Flierdt, T., Welsh, K., Yamane, M., 2013. Relative sea-level rise around East Antarctica during Oligocene glaciation. Nat. Geosci. 6, 380–384. https://doi.org/10.1038/ngeo1783.

Torsvik, T.H., Steinberger, B., Gurnis, M., Gaina, C., 2010. Plate tectonics and net lithosphere rotation over the past 150 My. Earth Planet. Sci. Lett. 291, 106–112. https://doi.org/10.1016/j.epsl.2009.12.055.

Vail, P.R., Mitchum, R.M., Thompson, S.I., 1977. Seismic Stratigraphy and Global Changes of Sea Level: Part 4. Global Cycles of Relative Changes of Sea Level Vol. 165, pp. 83–97.

Valdes, P.J., Scotese, C.R., Lunt, D.J., 2021. Deep ocean temperatures through time. Clim. Past 17, 1483–1506. https://doi.org/10.5194/cp-17-1483-2021.

van der Meer, D.G., Torsvik, T.H., Spakman, W., van Hinsbergen, D.J.J., Amaru, M.L., 2012. Intra-Panthalassa Ocean subduction zones revealed by fossil arcs and mantle structure. Nat. Geosci. 5, 215–219. https://doi.org/10.1038/ngeo1401.

van der Meer, D.G., Zeebe, R.E., van Hinsbergen, D.J.J., Sluijs, A., Spakman, W., Torsvik, T.H., 2014. Plate tectonic controls on atmospheric CO2 levels since the Triassic. Proc. Natl. Acad. Sci. 111, 4380–4385. https://doi.org/10.1073/pnas.1315657111.

van der Meer, D.G., van den Berg van Saparoea, A.P.H., van Hinsbergen, D.J.J., van de Weg, R.M.B., Godderis, Y., Le Hir, G., Donnadieu, Y., 2017. Reconstructing first-order changes in sea level during the Phanerozoic and Neoproterozoic using strontium isotopes. Gondwana Res. 44, 22–34. https://doi.org/10.1016/j.gr.2016.11.002.

van der Meer, D.G., van Hinsbergen, D.J.J., Spakman, W., 2018. Atlas of the underworld: Slab remnants in the mantle, their sinking history, and a new outlook on lower mantle viscosity. Tectonophysics 723, 309–448. https://doi.org/10.1016/j.tecto.2017.10.004.

Veizer, J., Prokoph, A., 2015. Temperatures and oxygen isotopic composition of Phanerozoic oceans. Earth-Sci. Rev. 146, 92–104. https://doi.org/10.1016/j.earscirev.2015.03.008.
Vellekoop, J., Sluijs, A., Smit, J., Schouten, S., Weijers, J.W.H., Damsté, J.S.S., Brinkhuis, H., 2014. Rapid short-term cooling following the Chicxulub impact at the Cretaceous-Paleogene boundary. Proc. Natl. Acad. Sci. 111, 7537–7541. https://doi.org/10.1073/pnas.1319253111.
Vellekoop, J., Esmeray-Senlet, S., Miller, K.G., Browning, J.V., Sluijs, A., van de Schootbrugge, B., Damsté, J.S.S., Brinkhuis, H., 2016. Evidence for Cretaceous-Paleogene boundary bolide "impact winter" conditions from New Jersey, USA. Geology 44, 619–622. https://doi.org/10.1130/G37961.1.
Vérard, C., Hochard, C., Baumgartner, P.O., Stampfli, G.M., Liu, M., 2015. 3D palaeogeographic reconstructions of the Phanerozoic versus sea-level and Sr-ratio variations. J. Paleogeogr. 4 (1), 64–84. https://doi.org/10.3724/SP.J.1261.2015.00072.
Vérard, C., Veizer, J., 2019. On plate tectonics and ocean temperatures. Geology 47, 881–885. https://doi.org/10.1130/G46376.1.
Vollstaedt, H., Eisenhauer, A., Wallmann, K., Böhm, F., Fietzke, J., Liebetrau, V., Krabbenhöft, A., Farkaš, J., Tomašových, A., Raddatz, J., Veizer, J., 2014. The Phanerozoic δ88/86Sr record of seawater: New constraints on past changes in oceanic carbonate fluxes. Geochim. Cosmochim. Acta 128, 249–265. https://doi.org/10.1016/j.gca.2013.10.006.
Von Bertalanffy, L., 1968. General Systems Theory. George Brazillier, New York.
Williams, S., Wright, N.M., Cannon, J., Flament, N., Müller, R.D., 2021. Reconstructing seafloor age distributions in lost ocean basins. Geosci. Front. 12, 769–780. https://doi.org/10.1016/j.gsf.2020.06.004.
Woodward, R.S., 1888. On the form and position of the sea level with special references to its dependence on superficial masses symmetrically disposed about a normal to the earth's surface (No. 48), Bulletin. Govt. Print. Off. https://doi.org/10.3133/b48.
Wright, N.M., Seton, M., Williams, S.E., Whittaker, J.M., Müller, R.D., 2020. Sea-level fluctuations driven by changes in global ocean basin volume following supercontinent break-up. Earth-Sci. Rev. 208,. https://doi.org/10.1016/j.earscirev.2020.103293 103293.
Yasheng, W.U., Jiasong, F.A.N., 2003. Quantitative Evaluation of the Sea-level Drop at the End-Permian: Based on Reefs. Acta Geol. Sin. - Engl. Ed. 77, 95–102. https://doi.org/10.1111/j.1755-6724.2003.tb00115.x.
Yin, H., Feng, Q., Lai, X., Baud, A., Tong, J., 2007. The protracted Permo-Triassic crisis and multi-episode extinction around the Permian-Triassic boundary. Glob. Planet. Change, Environ. Biotic Changes During Paleozoic-Mesozoic Transition 55, 1–20. https://doi.org/10.1016/j.gloplacha.2006.06.005.
Young, A., Flament, N., Maloney, K., Williams, S., Matthews, K., Zahirovic, S., Müller, R.D., 2019. Global kinematics of tectonic plates and subduction zones since the late Paleozoic Era. Geosci. Front., Special Issue: Adv. Himalayan Tectonics 10, 989–1013. https://doi.org/10.1016/j.gsf.2018.05.011.
Young, A., Flament, N., Williams, S.E., Merdith, A., Cao, X., Dietmar Müller, R., 2022. Long-term Phanerozoic sea level change from solid Earth processes. Earth Planet. Sci. Lett. 584,. https://doi.org/10.1016/j.epsl.2022.117451 117451.

**Douwe van der Meer** is a petroleum geoscientist specialized in plate tectonic processes and relation to tectono-stratigraphic evolution of basins. He has twenty years of petroleum-industry experience working for Shell and CNOOC/Nexen in the Netherlands, UK and USA, mainly focused on New Ventures exploration across the world. Following completion of his MSc. Geophysics at Utrecht University in 2002 and granting of his PhD. in 2017 cum laude, he has continued research in his spare time on mantle structure and the effect of plate tectonics on Earth's lithosphere, hydrosphere, and atmosphere.

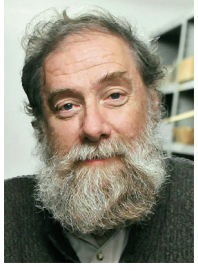

**Professor Christopher Scotese** retired from teaching at the University of Texas, Arlington, Department of Earth and Environmental Sciences in 2013. He is now a Research Associate at the Field Museum of Natural History and an Adjunct Professor in the Department of Earth and Environmental Sciences, Northwestern University. He continues to collaborate with several research groups on topics concerning the history of the Earth System, but his main focus is a book entitled: "Earth History, the Evolution of the Earth System". He is the coauthor of more than 100 scientific publications, and his maps and animations have been used in numerous geological textbooks, scientific research papers, and are on display in museums worldwide. Additional information can be found at the PALEOMAP website, the Global Geology website, Professor Scotese's YouTube channel, or his ResearchGate webpage.

**Benjamin J. W. Mills** is an Associate Professor at the University of Leeds, UK. He received a PhD in biogeochemical modelling in 2013 from the University of East Anglia. He builds models to understand the evolution of Earth's surface environment over geological time, specifically the processes which control planetary surface temperature and oxygenation of the atmosphere and oceans.

**Appy Sluijs** is professor of Paleoceanography at Utrecht University. He conducts research into climate changes in the geological past and into the relationship between CO2 and the Earth's climate, with a focus on the last 100 million years. He combines organic dinoflagellate cysts paleontology with (in)organic geochemical techniques, biogeological proxy development and modeling.

**Aart-Peter van den Berg van Saparoea** is a sedimentologist and petroleum geologist specialized in sequence stratigraphy and the architecture of clastic sedimentary systems. He has worked in the oil industry for fifteen years, primarily for various operators. Prior to this, as a post-doctoral researcher with the sedimentology group of Utrecht University, he studied the impact of high sediment supply on incision of continental shelves during sea level lowstands. This project was a continuation of his research as a PhD student with the same group, which was focused on the relative importance of external forcing mechanisms on the development and large-scale architecture of deltaic systems.

**Ruben van de Weg** is a Geomatics expert, specialized in GIS and Cartography. He has approximately 13 years of experience in the petroleum industry with NAM, Gasunie, BG Group and CNOOC-Nexen Petroleum UK, working within various assets of the industry such as environmental studies, exploration and development. His work mostly focusses on modelling, spatial data workflows, data governance, GIS application support, geomatics, Remote Sensing and GIS analysis. He has a keen interest in the application of GIS in geology and plate tectonics.